Numerical Simulation of Mass and Heat Transport Phenomena of Hydromagnetic Flow of Casson Fluid with Sinusoidal Boundary Conditions

by

Md. Rafiqul Islam
Department of Mathematics, Pabna University of Science and Technology, Pabna-6600, Bangladesh
Email: rafiqku.islam@pust.ac.bd; rafiqkuislam@gmail.com

Sk. Reza-E-Rabbi*
Mathematics Discipline, Khulna University, Khulna-9208, Bangladesh
Email: rabbi06@math.ku.ac.bd
ORCID id: https://orcid.org/0000-0002-4079-7507

Md. Yousuf Ali
Mathematics Discipline, Khulna University, Khulna-9208, Bangladesh
Email: yousufkumath@gmail.com

Md. Mehedi Hasan Rasel
Department of Mathematics and Natural Sciences, BRAC University, Mohakhali, Dhaka-1212, Bangladesh
Email: rasel1149083@gmail.com

Sarder Firoz Ahmmed
Mathematics Discipline, Khulna University, Khulna-9208, Bangladesh
Email: sfahmmed@math.ku.ac.bd

Author to whom correspondence may be addressed.
E-mail: *rabbi06@math.ku.ac.bd

Abstract

A computational study of Non-Newtonian (Casson) free convective MHD unsteady fluid flow has been highlighted in this article with mass and heat transit property through a vertical infinite porous plate. A sinusoidal boundary conditions have been considered as well as chemical reaction and thermal radiation. Using a collection of non-dimensional variables, the flow related equations are also turned into non-dimensional form. The EFDM algorithm is employed in order to arrive at a numerical solution via Compaq Visual Fortran 6.6a. The reliability of the numerical solution has been confirmed using stability testing and convergence analysis. The whole system is convergent at the value of $P_r \geq 0.075$ and $L_e \geq 0.025$. A visual depiction of the impact of the pertinent factors on dimensionless velocity, temperature, and concentration profiles is displayed along with thorough explanations and graphical representation as well as tabular representation. Key finding of this work is that when the magnetic component is regarded in sinusoidal form, it greatly affects the heat transfer factors of Casson fluid and the heat rises as the results of heat source parameter, radiation parameter and Eckert number. It is also found that the Sherwood number is increased as the impact of chemical reaction parameter and the Lewis number, also the skin friction is decreased as the influence of porosity term got accelerated. As a last step in verifying the earlier study, the present results are contrasted with the results that were previously published.

Keywords: Nanofluid, MHD, Thermal Radiation, Sinusoidal Boundary Conditions and Chemical Reaction.

1. Introduction

Convective heat transfer of magnetohydrodynamics flow has drawn a lot of interest due to its importance in the fields of research, technology, and several manufacturing processes In manufacturing industries like the extrusion of molten polymers, production of plastic sheets, solar power absorbs, thermal energy storage, etc., mixed convective flow through a porous surface is significant. The last few years have seen major advancements in the study of Magento-hydro dynamics in the fields of engineering and the natural sciences following Hartman's pioneering work. Numerous scientists are fascinated by the study of magneto-hydrodynamic fluid flow in a porous media that is not Newtonian due to its application to the processing of metals and alloys, the evaluation of geothermal sources, and the management of nuclear fuel debris. Magnetohydrodynamic (MHD) flows are crucial for a variety of industrial and technical applications including MHD generators, the architecture of nuclear reactor and flow meters. The study of how electrically conducting solutions move when a magnetic field is present is known as magnetohydrodynamics. The introduction of a magnetic phenomenon dramatically changes the mass transportation and heat transfer capabilities of common electrically conducting flows, according to a number of anticipated experiments. The study of magneto-hydro-dynamics has numerous important applications, including the induction pressure gauge, which depends on fluid potential differences orthogonal to motion and the magnetic field, and the cooling of nuclear power plants utilizing liquid sodium, among others. Due to different applications in scientific and technological advancements, the experiment of non- Newtonian laminar flow has garnered a lot of interest. A wide variety of sectors depend on materials, such as those used in petrochemical engineering and medicine. In addition, there are several uses in the manufacture of paints, syrups, oils, gases, juices, and cleansers, among other products. Additionally, a large number of other molten polymers and salt solutions, including starch suspensions, custard, toothpaste, ketchup, and shampoo, among others, are non-Newtonian fluids. A fluid's viscosity can change depending on how quickly it deforms, and certain fluids have an elastic component that makes them technically not fluids. Non-Newtonian fluid characteristics are challenging to analyze, as they differ from those of Newtonian fluids, and on those numerous applications, several scientists, researchers, and engineers have collaborated. Casson fluid's interaction between stress and strain makes it non-Newtonian in terms of rheological features. This fluid is a strong option for share thinning applications due to its high share viscosity and yield stress. The common Casson fluids are honey,

soup, jelly, concentrated fruit juices. It is very much significant in the field of petroleum industry, power generators, paints, purification of crude oil, heating of aerodynamics etc.

Under the impact of a first-order chemical transformation and the slip effect, the investigation by Saqib et al[1] looked at the methods by which mass and heat are transmitted while Casson fluid flows across an endless oscillating plate. They focused on researching the mechanics of the slip phenomenon near an edge of vertical plate and solved by Laplace transform technique. An unsteady boundary layer Casson fluid flow and heat transfer across a vertical plate that oscillates with Newtonian heating were investigated by Hussanan et al[2]. They recognized that as Casson parameters are increased, velocity drops, and thermal boundary layer thickness grows as a proportion of the Newtonian heating parameter. Rafique et al[3] by Keller-Box Method, determined a numerical solution for the Casson nanofluid flow over such an inclination surface that is not linear with the impacts of Soret and Dufour. They claimed that the Dufour effect lowers the Nusselt and Sherwood number as a result of the Soret influence. Again, for exponentially permeable surface Raju et al[4] used MATLAB bvpc package for numerical simulating the mass and heat transit of MHD flow of Casson fluid. They compared to Newtonian fluid, Casson fluid has superior heat transfer capability. Recently, MHD Casson fluid flow study over a permeable stretching sheet with heat and mass transfer was carried out by Asogwa et al[5]. Numerical approach was performed by MATLAB bvpc solver in their paper. The influence of heat radiation and chemical reaction on the MHD non-Newtonian (Casson fluid) flow across an increasingly sloped stretched surface were also documented by Rao et al[6] in their study. A widely used shooting method was taken for numerical calculation. Study with the chemical reaction-related MHD radiant mobility of Casson and Williamson nanofluids along an inclination surface which was cylindrical was interpreted by Sarker et al[7]. FDM was applied for numerical approach. Ullah et al[8] developed another Casson fluid in an unsteady MHD slip flow with mixed convection over a nonlinearly extending sheet. The Keller box approach was used to a numerical simulation of a porous media containing thermal radiation, heat generation/absorption, chemical reaction, and convective boundary conditions. Recently, Hasnain et al[9] inspected the investigation of sand-filled Casson fluid flow bearing power laws for temperature and magnetic field over a permeable stretching sheet. Also, Pramanik et al[10] analyzed heat transfer and fluid flow of non-Newtonian (Casson) fluid through a porous stretched surface which expand with exponentially by using numerical technique. They figured out the effects brought about by heat radiation and suction/blowing combinedly. Recently, Oke et al[11]

investigated the behavior of Casson fluid flow on a non-uniform spinning surface because of Coriolis force. They have been using the Runge-Kutta-Gills strategy with the financial support of the shooting technique for their research and investigation of the significance of Coriolis force as the properties of Casson fluid flow through the non-uniform thickness surface. Sulochona et al[12] addressed Casson fluid flowing with an unsteady MHD rate through vertical plate with exist of Hall current. Perturbation technique was used for analytical analysis. Two non-Newtonian Casson solutions for fluid flow and heat transfer across an exponentially permeable shrinking sheet with viscous dissipation exist was developed by Zaib et al[13]. Sohail et al[14] researched entropy generation of magnetized flow of Casson fluid through non-linear bi-directional stretching surface with variable heat conductance and thermal conductivity. A proficient numerical technique optimal homotopy analysis method (OHAM) was used in their paper. Mondal et al[15] provided a simulation on MHD flow of Casson fluid with varying viscosity and thermal conductivity characteristics. For additional analysis in this study, the explicit finite difference method was applied. Abro et al[16] published a research work on mathematical analysis of the Casson fluid flow under magnetic field using unique functions with embedded heat and mass transport. By using newly developed generalized Robotnov-Hartley, Wright, and Mittage-Leffler functions, they correspondingly presented the relevant results of mass concentration, temperature distribution, and velocity profiles. However, Prameela et al[17] demonstrated free convective MHD fluid flow with non-Newtonian (Casson) phenomena across a vertical plate oscillating. Numerical investigations were conducted by employing Finite Element approach. Ogunseye et al[18] presented a computational analysis of the mass and heat transferred by a reactive Casson-Williamson nanofluid via a moveable cylinder in the vertical direction and they develop a ground-breaking bivariate overlapping multi-domain technique using the spectral quasi-linearization method for analyzing non - dimensional mathematical nonlinear specified flow equations in their article. Recently, a stretchy electromagnetic plate that affects the dynamics of the MHD Casson nanofluid in aspects of radiation, chemical reaction, and suction was produced by Asogwa et al[19] by imposing a stagnation point flow. MATLAB bvp4c was used for numerical result. On the extending Riga surface, they discovered that chemical reaction increased while, on the other hand, the thickness of the concentration boundary layer decreased due to Lewis number and Brownian motion. Khalid et al[20] demonstrated the turbulent MHD free convection of Casson fluid via a rotating vertical plate enclosed in a porous substance. Kumar et al[21] explored the consequences of cross diffusion in

Casson fluid nonlinear radiative heat transfer and MHD mixed convection flow over a vertical plate. They resolved the system of equations numerically with the help of RKF45 Method along with shooting method and discovered that the temperature and concentration component rise in accordance with the influence of the Dufour and Soret parameter. Qayyum et al[22] expressed slip analysis via porous media at the fluid-solid boundary of squeezing flow in MHD Casson fluid. Using FEM, over a vertical plate that is oscillating, impacts of viscous dissipation was expressed by Reddy et al[23] on flow of a viscous MHD fluid in an unstable condition with spontaneous convection. They employed the computational FEM to obtain boundary layer PDE's as non-dimensional form. Skin friction is very much important for industry. They found that the fall of velocity distribution and the Skin-friction coefficient due to increasing of Casson. Recently, with inclined non-linear surface thermal energy impacts on Casson fluid which was magnetized using a non-linear inclined surface Forchheimer porous medium was presented by Shoaib et al[24]. The Levenberg Marquardt algorithm was choose, together with a backpropagated learning mechanism to obtain numerical outcomes. Their key finding is the temperature profile drops for the rise of Forchheimer porous media parameter. Moreover, Effect of radiation on MHD Bejawada et al[25] modeled Casson (non-Newtonian) fluid flow over an elevated non-linear surface including chemical reaction in a Forchheimer porous medium. They solved the coupled ordinary differential equation by using Runge-Kutta method along with the shooting technique. It was discovered that the plate's temperature drops as the value of Forchheimer porous medium parameter rises. Kataria et al[26] developed combined effects of radiation and chemical reaction on MHD Casson fluid flow through a vertical plate that is in motion was embedded in porous medium with analytic solution using Laplace transform technique. It has been discovered that when heat radiation climbs, velocity increases and temperature falls. The Casson fluid flow with changeable thermo-physical properties including suction along an exponentially stretched sheet and exponentially declining internal heat production were described by Animasaun et al[27] using homotopy analysis. To demonstrate the impact of several relevant parameters on the fluid velocity and temperature profiles within the boundary layer, they developed a parametric research. In addition, recently thermal features and heat transfer enhancement of a Casson fluid across a porous stretching/shrinking sheet: Analysis of dual solutions was presented by Khan et al[28]. Utilizing MATLAB's bvp4c tool, the dual solutions for the dimensionless ODEs have been found. They discovered that, although declining with increased heat generation parameter, the heat transfer rate improved with increased radiation,

Biot number, and Prandtl number. Hussain et al[29] provided a thermal analysis of a gold nanoparticle-containing Casson rheological fluid under the effect of magnetic and gravitational forces. They found that through the inclined channel, magnetized Newtonian particulate suspension is more prominent. Zhou et al[30] analyzed unsteady convective slip flow of the MHD Casson fluid across a stretched permeable surface that was simultaneously being heated unevenly. The MATLAB bvp4c function also employed to calculate the system of ODEs. With rising levels of the porosity parameter and inclination angle, the velocity profiles decrease. In addition, Darcy Forchheimer variation in Casson type MHD nanofluid flow across non-linear stretching surface was examined by Rasool et al[31]. Raju et al[32] figured out MHD Casson fluid in a suspension of convective conditions and cross diffusion across a surface of paraboloid of revolution. They discovered that mixed convective circumstances are beneficial for enhancing the mass and heat transfer phenomena. Thermal radiation, viscous dissipation, and heat sources/sinks are present during the MHD flow of a Casson fluid with slip effects across an exponentially porous stretched sheet was discussed by Saidulu et al[33]. They also used the keller box method. Reza-E-Rabbi et al[34] studied out the investigation of heat transfer and fluid flow of a periodic MHD nano non-Newtonian fluid with Arrhenius activation energy and nonlinear radiation. They applied the explicit finite difference (EFD) approach for further analysis. Anwar et al[35] introduced unsteady MHD Casson fluid flow with natural convection of combining heat injection/suction and thermal radiation flux with varying wall constraints. They solved the coupled ordinary differential equations by dint of Laplace transform technique. Moatimid et al[36] look at the Casson nanofluid flow phenomena in the conical gap between the rotating surfaces of a cone and a horizontal disc. The Homotopy perturbation method is implemented to analytically evaluate the systems of equations. They discovered that the fluid's temperature and radial velocity both decrease as a result of the rotational parameters. Ahmad et al[37] used Fick’s and Fourier’s Laws for time fractional analysis of channel flow of couple stress Casson fluid. Production of entropy in MHD For non-linear bi-directional stretching surfaces, Sohail et al[38] described Casson fluid flow with variable thermal conductivity and heat conductance. They showed the solutions by implementing the optimal homotopy analysis method (OHAM). In order to examine the combined Hall current and heat radiation hydromagnetic flow of a Casson nanofluid, Sahoo[39] constructed an analysis of entropy production and dissipative heat transfer. An efficient spectral quasi-linearization method was applied for numerical analysis. In addition, Shah et al[40] expressed over a previously

nonlinearly stretched surface, a radiative MHD Casson nanofluid flowed with activation energy and chemical reaction through entropy generation. For the evaluation of results homotopy analysis method was applied. They figured out that activation energy corresponds to augmented concentration. Kataria and Patel[41] analyzed Heat and mass transfer in magnetohydrodynamic Casson fluid flow over an oscillating plate which placed as vertically and also embedded in porous medium with ramped wall temperature. A numerical investigation on the pulsating flow of a micropolar-Casson fluid through a constrained channel driven by a magnetic field and a Darcian porous medium was presented by Ali et al[42]. When nonlinear radiation and convective boundary conditions were present, Hussain et al[43] conducted MHD thermal boundary layer flow of a Casson fluid across a penetrable stretched wedge. They applied Homotopy analysis method (HAM). Additionally, Nandeppanavar et al[44] expressed an examination of the thermal properties of a Casson nanofluid flowing past an exponential stretching sheet in a porous medium using theoretical methods.

Motivated from the aforementioned studies, heat and mass transform on MHD free convective Casson fluid flow with unsteady form past in an infinite vertical porous plate in the presence of radiation and chemical reaction with sinusoidal boundary conditions was investigated. The momentum equation includes the influence of magnetic force, whereas the energy equation incorporates the effects of heat radiation. Using the appropriate similarity methodology, the leading coupled nonlinear PDE's are reduced into ODE'. The explicit finite difference strategy is utilized to numerically solve these nonlinear ordinary differential equations. Plotted graphs and tables are used to analyze and discuss the many parameters of the present flow problem in detail. For sinusoidal boundary conditions, when the radiating heat flux is taken into account, the Lorentz force for magnetic parameters has reduced the flow profiles. The impacts of Grashof number and radiation parameter have been encapsulated by the advanced visualizations better known as streamlines and isotherms for flow fields. Table 1 has been specifically made to show how the current approach contrasts with prior published research in the field.

TABLE 1.

Authors	NNF	MHD	RP	HSP	CR	NF	PT
Raju et al[4]	Yes	Yes	Yes	Yes	Yes	No	No
Asogwa et al[5]	Yes	Yes	Yes	No	Yes	No	No
Sarkar et al[7]	Yes	Yes	Yes	No	Yes	Yes	No
Ullah et al[8]	Yes	Yes	Yes	No	Yes	No	Yes
Sulochana et al[12]	Yes	Yes	Yes	Yes	Yes	No	No
Reza-E-Rabbi et al[34]	Yes	Yes	Yes	Yes	No	Yes	No
Current work	Yes	Yes	Yes	Yes	Yes	Yes	Yes

Abbreviations: NNF (Non-Newtonian Fluid); MHD (Magnetohydrodynamics); RP (Radiation Parameter); NF (Nano Fluid); HSP (Heat Source Parameter); CR (Chemical Reaction); PT (Porous Term).

Applications

The present research has applications across a wide range of technical fields, including the creation of thermal nanotechnology components. Additionally, control of heat transmission in the polymer production business must depend on the thermal radiation component. High temperatures then lead to the development of a variety of novel technical processes, including solar energy technology and energy technologies based on the combustion of fossil fuels. Therefore, it would appear crucial to study heat radiation. Here, thermal radiation with linear patterns have been thoroughly investigated. The treatment of prostate cancer is one area where the recent study has application. Magnetic fields frequently help to regulate the drug's particle emission, which is one application of nanoparticles in the treatment of cancer.

2. Methodology

Influenced by prior research and experiences as well as the magnificence of nanofluid and MHD exploration, this investigation depicts the effects of chemical reaction as well as radiation on unsteady MHD nanofluids moving towards sinusoidal boundary conditions. This research, which is based on a numerical simulation, must be completed with the use of an effective numerical technique. This leads to the use of the EFD (Explicit Finite Difference) procedure. The biggest benefit of adopting an explicit finite approach is how much faster it computes. Computing-wise, the process is comparatively quick and affordable. In spite of this, making it work and programming it are fairly simple. As soon as the approach is implemented, a stability test is conducted, which clarifies the problem. The structure of the present project is as follows:

- A collection of fundamental equations, including continuity, momentum, and energy equations, have been developed using the fundamental concept of fluid mechanics.
- A number of dimensionless components are used to make the produced equations non-dimensional. The suggested equations are numerically resolved using the EFD method.
- To guarantee that the solution converges, a thorough stability and convergence criteria has been constructed.
- A program named Visual Fortran is used to acquire the numerical data.
- The graphical depiction and evaluation of the numerical data are done using Tecplot 9.0.
- Finally, the findings and discussion section compare the traditional form of various flow fields with the velocity, isothermal, and streamline profiles which all are sinusoidal form. Here, it has been looked at how physically different parameters are.

Methodology of the problem can be depicted through the following flow chart,

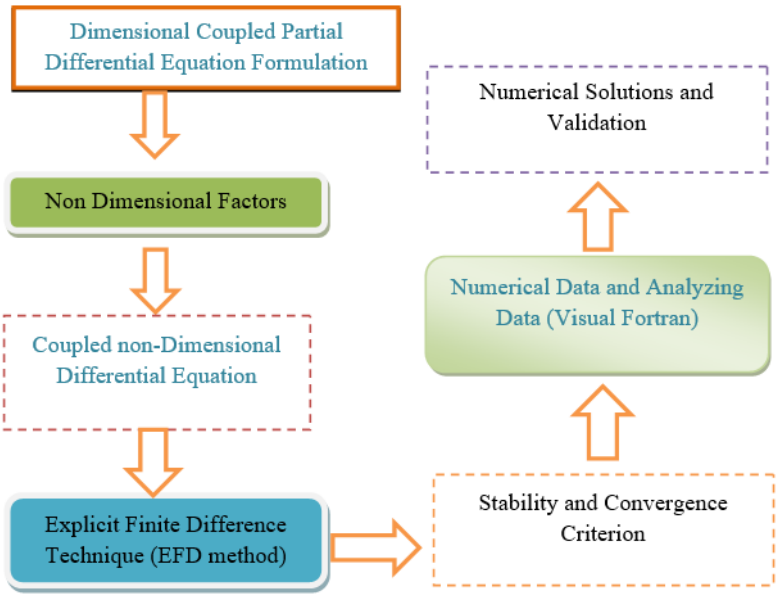

FIGURE 1. Flow chart (Methodology).

3. Mathematical Analysis

The MHD unsteady Casson nanofluid flow with mass and heat transformation through in a vertical porous plate which is taken as infinite is explored in this paper with existing the Chemical reaction and Radiation. The sinusoidal conditions $1+A\sin\pi x$ is taken with wall temperature and C_w is taken as concentration near the wall, respectively at $t>0$. As opposed to, T and C are the fluid

temperature and Concentration at everywhere. Now for the Casson nanofluid flow, the rheological equation is underived,

$$\pi_{ij} = \begin{cases} \left(\mu_c + \dfrac{P_y}{\sqrt{2\pi}}\right)2\zeta_{ij} & \text{when } \pi > \pi_b \\ \left(\mu_c + \dfrac{P_y}{\sqrt{2\pi_b}}\right)2\zeta_{ij} & \text{when } \pi < \pi_b \\ \text{where, } P_y = \mu_c\sqrt{2\pi}\beta^{-1} \end{cases};$$

$$\therefore \upsilon' = \upsilon\left(1+\beta^{-1}\right) \text{ where, } \upsilon = \mu_c\rho^{-1}$$

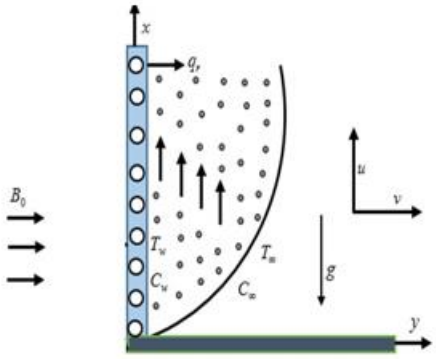

FIGURE 2. Physical diagram and Coordinate system.

Here, ζ_{ij} and π_{ij} are $(i, j)^{\text{th}}$ factor of the deformation rate and the stress tensor, respectively, μ_c is the plastic dynamic viscosity of the Casson fluid, π represents the product of the component of deformation rate with itself, π_b denoted the critical value of this product, and P_y indicates the yield stress of fluid.

Now, by applying the boundary layer approximation and under the above consideration the system of governing equations of the Magneto-hydro-dynamics nanofluid flow is provided by

Continuity Equation

$$\frac{\partial u}{\partial x} = -\frac{\partial v}{\partial y} \tag{1}$$

Momentum Equation

$$\frac{\partial u}{\partial t} = \upsilon\left(1+\beta^{-1}\right)\frac{\partial^2 u}{\partial y^2} + g\beta_T(C-C_\infty) + g\beta_T(T-T_\infty) - \frac{\sigma B_0^2 u}{\rho} - \left(1+\beta^{-1}\right)\frac{\upsilon}{k}u - \left(u\frac{\partial u}{\partial x} + v\frac{\partial u}{\partial y}\right) \tag{2}$$

Energy Equation

$$\frac{\partial T}{\partial t} = \frac{k}{\rho c_p}\frac{\partial^2 u}{\partial y^2} + (1+\beta^{-1})\frac{\upsilon}{\rho c_p}\left(\frac{\partial u}{\partial y}\right)^2 + \tau\left[\frac{D_T}{T_\infty}\left(\frac{\partial T}{\partial y}\right)^2 + D_B\left(\frac{\partial T}{\partial y}\frac{\partial C}{\partial y}\right)\right] - \left(u\frac{\partial T}{\partial x} + v\frac{\partial T}{\partial y}\right) - \frac{1}{\rho c_p}\frac{\partial q_r}{\partial y} + \frac{Q_0}{\rho c_p}\left(T-T_\infty\right) \tag{3}$$

Concentration Equation

$$\frac{\partial C}{\partial t} = D_B \frac{\partial^2 C}{\partial y^2} + \frac{D_T}{T_\infty}\frac{\partial^2 T}{\partial y^2} - \left(u\frac{\partial C}{\partial x} + v\frac{\partial C}{\partial y} \right) - K_c (C - C_\infty)^p \tag{4}$$

Initial and boundary criteria that match are

$$\left.\begin{array}{ll} t = 0,\ C = C_\infty,\ T = T_\infty,\ u = 0,\ v = 0 & \text{everywhere} \\ t \geq 0,\ C = C_\infty,\ T = T_\infty,\ u = 0,\ v = 0 & \text{at}\quad x = 0 \\ u = U_0,\ v = 0,\ T = T_\infty + (T_w - T_\infty)(1 + A\sin \pi x),\ C = C_w & \text{at}\quad y = 0 \\ C \to C_\infty,\ T \to T_\infty,\ u = 0,\ v = 0 & \text{as}\quad y \to \infty \end{array}\right\} \tag{5}$$

Where, u and v indicate the velocity components, β be the Casson term, the magnetic field component is defined by B_0, β_T and β_C are the thermal and concentration expansion coefficient, the wall temperature and the species wall concentration are represent by T_w and C_w, υ indicates the kinematic viscosity, the density, thermal conductivity, specific heat at constant pressure and unidirectional radiative heat flux are defined by ρ, κ, c_p and q_r, respectively. D_B and D_T are the Brownian and thermophoresis diffusion coefficient. The Rosseland approximation becomes, $q_r = -\dfrac{4\tilde{\sigma}}{3k_s}\dfrac{\partial T^4}{\partial y}$ for radiative heat flux. Expanding T^4 by Tailor's approximation at T_∞, we get $T^4 \approx 4T_\infty^3 T - 3T_\infty^4$. (By neglecting the Higher ranked terms because of its small value). The equation (3) become,

$$\begin{aligned} \frac{\partial T}{\partial t} = {} & \frac{k}{\rho c_p}\frac{\partial^2 u}{\partial y^2} + (1 + \beta^{-1})\frac{\upsilon}{\rho c_p}\left(\frac{\partial u}{\partial y}\right)^2 + \tau\left[D_B\left(\frac{\partial C}{\partial y}\frac{\partial T}{\partial y}\right) + \frac{D_T}{T_\infty}\left(\frac{\partial T}{\partial y}\right)^2 \right] - u\frac{\partial T}{\partial x} - v\frac{\partial T}{\partial y} \\ & + \frac{16\tilde{\sigma}T_\infty^3}{3k_s\rho c_p}\frac{\partial^2 T}{\partial y^2} + \frac{Q_0}{\rho c_p}(T - T_\infty) \end{aligned} \tag{6}$$

Dimensionless equations must be used because the finite difference technique will be used to solve the governing equations (1) through (4) under the boundary conditions (5). For this intention the non-dimensional components listed below,

$$X = \frac{xU_0}{\upsilon}, U = \frac{u}{U_0}, Y = \frac{yU_0}{\upsilon}, V = \frac{v}{U_0}, \tau = \frac{tU_0^2}{\upsilon}, \phi = \frac{C - C_\infty}{C_w - C_\infty}, \theta = \frac{T - T_\infty}{T_w - T_\infty} \tag{7}$$

In terms of non-dimensional variables, the following system of partial differential equations with nonlinearity is produced:

$$\frac{\partial U}{\partial Y}+\frac{\partial U}{\partial X}=0 \tag{8}$$

$$\frac{\partial U}{\partial \tau}+V\frac{\partial U}{\partial Y}+U\frac{\partial U}{\partial X}=\left(1+\beta^{-1}\right)\frac{\partial^2 U}{\partial Y^2}-MU-\left(1+\beta^{-1}\right)K_p U+G_r\theta+G_m\phi \tag{9}$$

$$\frac{\partial \theta}{\partial \tau}+U\frac{\partial \theta}{\partial X}+V\frac{\partial \theta}{\partial Y}=N_b\left(\frac{\partial \theta}{\partial Y}\frac{\partial \phi}{\partial Y}\right)+\frac{(1+R_d)}{P_r}\frac{\partial^2 \theta}{\partial Y^2}+N_t\left(\frac{\partial \theta}{\partial Y}\right)^2+\left(1+\beta^{-1}\right)\left(\frac{\partial U}{\partial Y}\right)^2 E_c+Q\theta \tag{10}$$

$$\frac{\partial \phi}{\partial \tau}+U\frac{\partial \phi}{\partial X}+V\frac{\partial \phi}{\partial Y}=\frac{1}{L_e}\left[\frac{N_t}{N_b}\left(\frac{\partial^2 \theta}{\partial Y^2}\right)+\frac{\partial^2 \phi}{\partial Y^2}\right]-K_r\left(\phi\right)^p \tag{11}$$

With matching initial and boundary conditions are

$$\left.\begin{array}{ll}
\tau\le 0,\ \phi=0,\ U=0,\quad \theta=0,\ V=0 & \text{everywhere}\\
\tau>0,\ \phi=0,\ U=0,\quad \theta=0,\ V=0 & \text{at}\quad X=0\\
\phi=1,\ \theta=1+A\sin\pi X,\ V=0,\ U=1, & \text{at}\quad Y=0\\
\phi\to 0\ ,\ \theta\to 0,\quad U=V=0, & \text{as}\quad Y\to\infty
\end{array}\right\} \tag{12}$$

The dimensionless parameters such as Thermal Grashof number, Magnetic parameter, Mass Grashof number, Radiation parameter, Prandtl number, Lewis number, Brownian parameter r, Eckert number, porous term, Thermophoresis parameter, Heat source parameter and Chemical reaction are defined by

$$G_r=\frac{g\beta_T(T_w-T_\infty)\upsilon}{U_0^3},\ M=\frac{\sigma B_0^2\upsilon}{\rho U_0^2},\ G_m=\frac{g\beta_C(C_w-C_\infty)\upsilon}{U_0^3},\ R_d=\frac{16\tilde{\sigma}T_\infty^3}{3\kappa k_s},\ P_r=\frac{\upsilon\rho c_p}{\kappa},\ L_e=\frac{\upsilon}{D_B},$$

$$N_b=\frac{\tau D_B(C_w-C_\infty)}{\upsilon},\quad E_c=\frac{U_0^2}{c_p(T_w-T_\infty)},\quad K_p=\frac{\upsilon^2}{k_s U_0^2},\quad N_t=\frac{\tau D_T(T_w-T_\infty)}{\upsilon T_\infty},\quad Q=\frac{Q_0\upsilon}{\rho c_p U_0^2}$$

$$K_r=\frac{k_s\upsilon(C_w-C_\infty)^{p-1}}{U_0^2}.$$

The velocity components in the terms of stream function are $U=\frac{d\psi}{dY}$ and $V=-\frac{d\psi}{dX}$, where Stream function ψ satisfies the continuity equation (8).

The important physical phenomena of the fluid flow are skin-friction coefficient, the Sherwood number and the Nusselt number, things are outlined below $C_f = -\frac{1}{2\sqrt{2}}\left(1+\beta^{-1}\right)\left(\frac{\partial U}{\partial Y}\right)_{Y=0}$, $S_h = \frac{1}{\sqrt{2}L_e}\left(\frac{\partial \phi}{\partial Y}\right)_{Y=0}$ and $N_u = \frac{1}{\sqrt{2}P_r}\left(1+R_d\right)\left(\frac{\partial \theta}{\partial Y}\right)_{Y=0}$.

4. Numerical Solutions

In this section, we attempt to solve numerically the governing dimensionless partial differential equations by using the EFD (Explicit Finite Difference) with the flow related initial and boundary conditions.

In order to calculate the finite difference equations, the flow zone is divided by a grid or mesh of lines that are perpendicular to the *X* and *Y* axes and measured along the *X* and *Y* axes, respectively. Here, we assume that the plate has a maximum height of X_{max}(=100), i.e., *X* varies between 0 and 100, and we consider Y_{max}(=25) to equate to *Y* varying between 0 and 25.

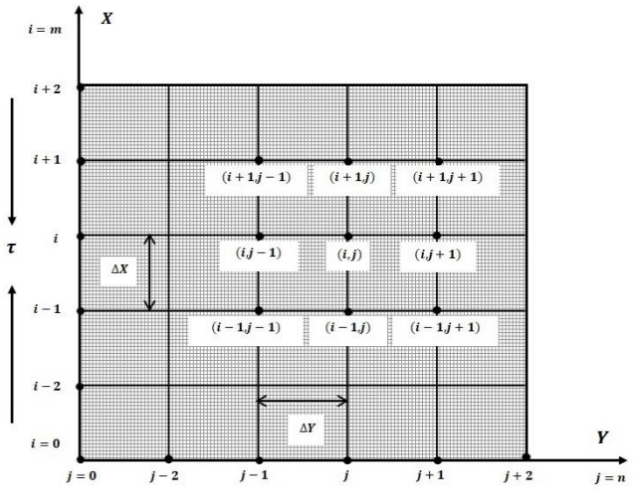

FIGURE 3. Finite difference space grid.

According to Fig. 2, there are grid spacings of *m* = 125 and *n* = 125 in the *X* and *Y* axes, respectively. Let ΔX, ΔY are the constant mesh size in the *X* and *Y* dimensions, the following is taken into consideration:

$\Delta Y = 0.2(0 \le x \le 25); \Delta X = 0.8(0 \le x \le 100)$ utilizing the shorter time-step, $\Delta\tau = 0.0005$.

Let us consider $\tilde{U},\tilde{\theta}$ and $\tilde{\phi}$ stand for the respective values of U,θ and ϕ at the conclusion of a time-step. We get the following from the explicit finite difference approximation,

$$\left(\frac{\partial U}{\partial X}\right)_{i,j}=\frac{U_{i,j}-U_{i-1,j}}{\Delta X},\ \left(\frac{\partial U}{\partial \tau}\right)_{i,j}=\frac{\tilde{U}_{i,j}-U_{i,j}}{\Delta \tau},\ \left(\frac{\partial U}{\partial Y}\right)_{i,j}=\frac{U_{i,j+1}-U_{i,j}}{\Delta Y},\ \left(\frac{\partial V}{\partial Y}\right)_{i,j}=\frac{V_{i,j}-V_{i,j-1}}{\Delta Y},$$

$$\left(\frac{\partial \theta}{\partial Y}\right)_{i,j}=\frac{\theta_{i,j+1}-\theta_{i,j}}{\Delta Y},\ \left(\frac{\partial \theta}{\partial X}\right)_{i,j}=\frac{\theta_{i,j}-\theta_{i-1,j}}{\Delta X},\ \left(\frac{\partial \theta}{\partial \tau}\right)_{i,j}=\frac{\tilde{\theta}_{i,j}-\theta_{i,j}}{\Delta \tau}$$

$$\left(\frac{\partial \phi}{\partial Y}\right)_{i,j}=\frac{\phi_{i,j+1}-\phi_{i,j}}{\Delta Y},\ \left(\frac{\partial \phi}{\partial \tau}\right)_{i,j}=\frac{\tilde{\phi}_{i,j}-\phi_{i,j}}{\Delta \tau},\ \left(\frac{\partial \phi}{\partial X}\right)_{i,j}=\frac{\phi_{i,j}-\phi_{i-1,j}}{\Delta X} \tag{13}$$

$$\left(\frac{\partial^2 \theta}{\partial Y^2}\right)_{i,j}=\frac{\theta_{i,j+1}-2\theta_{i,j}+\theta_{i,j-1}}{(\Delta Y)^2},\left(\frac{\partial^2 U}{\partial Y^2}\right)_{i,j}=\frac{U_{i,j+1}-2U_{i,j}+U_{i,j-1}}{(\Delta Y)^2},\left(\frac{\partial^2 \phi}{\partial y^2}\right)_{i,j}=\frac{\phi_{i,j+1}-2\phi_{i,j}+\phi_{i,j-1}}{(\Delta Y)^2}$$

We construct a suitable set of finite difference equations from the system of PDE's (8–11) by substituting the aforementioned relations into the respective differential equation,

$$\frac{U_{i,j}-U_{i-1,j}}{\Delta X}=\frac{V_{i,j-1}-V_{i,j}}{\Delta Y} \tag{14}$$

$$\frac{\tilde{U}_{i,j}-U_{i,j}}{\Delta \tau}=\left(1+\beta^{-1}\right)\frac{U_{i,j+1}-2U_{i,j}+U_{i,j-1}}{(\Delta Y)^2}+G_r\theta_{i,j}+G_m\phi_{i,j}-MU_{i,j}$$
$$-V_{i,j}\frac{U_{i,j+1}-U_{i,j}}{\Delta Y}-U_{i,j}\frac{U_{i,j}-U_{i-1,j}}{\Delta X}-\left(1+\beta^{-1}\right)K_pU_{i,j}$$

$$\therefore \tilde{U}_{i,j}=U_{i,j}+\Delta\tau\left[G_r\theta_{i,j}+G_m\phi_{i,j}+\left(1+\beta^{-1}\right)\frac{U_{i,j+1}-2U_{i,j}+U_{i,j-1}}{(\Delta Y)^2}-MU_{i,j}-\left(1+\beta^{-1}\right)K_pU_{i,j}\right] \tag{15}$$
$$-\Delta\tau\left[U_{i,j}\frac{U_{i,j}-U_{i-1,j}}{\Delta X}+V_{i,j}\frac{U_{i,j+1}-U_{i,j}}{\Delta Y}\right]$$

$$\frac{\tilde{\theta}_{i,j}-\theta_{i,j}}{\Delta \tau}=N_t\left(\frac{\theta_{i,j+1}-\theta_{i,j}}{\Delta Y}\right)^2+\left(\frac{1+R_d}{\mathrm{P_r}}\right)\frac{\theta_{i,j+1}-2\theta_{i,j}+\theta_{i,j-1}}{(\Delta Y)^2}+N_b\frac{\theta_{i,j+1}-\theta_{i,j}}{\Delta Y}\frac{\phi_{i,j+1}-\phi_{i,j}}{\Delta Y}$$
$$-V_{i,j}\frac{\theta_{i,j+1}-\theta_{i,j}}{\Delta Y}+\left(1+\beta^{-1}\right)E_c\left(\frac{U_{i,j+1}-U_{i,j}}{\Delta Y}\right)^2-U_{i,j}\frac{\theta_{i,j}-\theta_{i-1,j}}{\Delta X}$$

$$\therefore \tilde{\theta}_{i,j} = \Delta\tau\left[N_b \frac{\theta_{i,j+1}-\theta_{i,j}}{\Delta Y}\frac{\phi_{i,j+1}-\phi_{i,j}}{\Delta Y} + \left(\frac{1+R_d}{\mathrm{P_r}}\right)\frac{\theta_{i,j+1}-2\theta_{i,j}+\theta_{i,j-1}}{(\Delta Y)^2} + N_t\left(\frac{\theta_{i,j+1}-\theta_{i,j}}{\Delta Y}\right)^2\right] + \theta_{i,j}$$
$$-\Delta\tau\left[V_{i,j}\frac{\theta_{i,j+1}-\theta_{i,j}}{\Delta Y} - \left(1+\beta^{-1}\right)E_c\left(\frac{U_{i,j+1}-U_{i,j}}{\Delta Y}\right)^2 + U_{i,j}\frac{\theta_{i,j}-\theta_{i-1,j}}{\Delta X}\right] \quad (16)$$

$$\frac{\tilde{\phi}_{i,j}-\phi_{i,j}}{\Delta\tau} = \frac{N_t}{N_b L_e}\left(\theta_{i,j+1}-2\theta_{i,j}+\theta_{i,j-1}\right)(\Delta Y)^{-2} + \frac{1}{L_e}\left(\phi_{i,j+1}-2\phi_{i,j}+\phi_{i,j-1}\right)(\Delta Y)^{-2}$$
$$+V_{i,j}\left(\phi_{i,j}-\phi_{i,j+1}\right)(\Delta Y)^{-1} + U_{i,j}\left(\phi_{i-1,j}-\phi_{i,j}\right)(\Delta X)^{-2} - K_r\left(\phi_{i,j}\right)^p$$

$$\therefore \tilde{\phi}_{i,j} = \Delta\tau\left[(L_e)^{-1}\left(\phi_{i,j+1}-2\phi_{i,j}+\phi_{i,j-1}\right)(\Delta Y)^{-2} + \frac{N_t}{N_b L_e}\left(\theta_{i,j+1}-2\theta_{i,j}+\theta_{i,j-1}\right)(\Delta Y)^{-2}\right] + \phi_{i,j}$$
$$-\Delta\tau\left[V_{i,j}\left(\phi_{i,j+1}-\phi_{i,j}\right)(\Delta Y)^{-1} + U_{i,j}\left(\phi_{i,j}-\phi_{i-1,j}\right)(\Delta X)^{-1} + K_r\left(\phi_{i,j}\right)^p\right] \quad (17)$$

Corresponding boundary conditions are

$$\left.\begin{array}{lll} U_{i,S}^n = \phi_{i,S}^n = 1; & \theta_{i,S}^n = 1 + A\sin\pi X, & \text{where } S = 0 \\ U_{i,S}^n = \phi_{i,S}^n = 0; & \theta_{i,S}^n = 0, & \text{where } S \to \infty \end{array}\right\} \quad (18)$$

4.1. Stability and Convergence Analysis

The analysis won't be complete because an explicit approach is being employed until we discuss how the finite difference approach converges and remains stable. The stability conditions of the scheme may be established as follows for constant mesh sizes.

Apart from a constant, the basic terms for U, θ and ϕ as the Fourier expansion at a time conventionally called $\tau = 0$ are all $e^{i\alpha X}e^{i\beta Y}$, where $i = \sqrt{-1}$. These words eventually become

$$\left.\begin{array}{ll} U: & D(\tau)e^{i\beta Y}e^{i\alpha X} \\ \theta: & E(\tau)e^{i\alpha X}e^{i\beta Y} \\ \phi: & F(\tau)e^{i\beta Y}e^{i\alpha X} \end{array}\right\} \quad (19)$$

and following the time-step, these words will change to

$$\left.\begin{array}{ll}\tilde{U}: & \tilde{D}(\tau)e^{i\beta Y}e^{i\alpha X}\\ \tilde{\theta}: & \tilde{E}(\tau)e^{i\beta Y}e^{i\alpha X}\\ \tilde{\phi}: & \tilde{F}(\tau)e^{i\alpha X}e^{i\beta Y}\end{array}\right\} \tag{20}$$

Substituting (19) and (20) into equations (14) – (17), we get the following equations by treating for each particular time step, the coefficients of *U* and *V*,

$$\frac{e^{i\beta Y}\left(\tilde{D}-D\right)e^{i\alpha X}}{\Delta\tau}=\left(1+\beta^{-1}\right)\frac{2e^{i\beta Y}De^{i\alpha X}\left(\cos\beta\Delta Y-1\right)}{\left(\Delta Y\right)^2}+G_r e^{i\alpha X}Ee^{i\beta Y}+G_m e^{i\beta Y}Fe^{i\alpha X}$$

$$-Me^{i\beta Y}De^{i\alpha X}-V\frac{De^{i\beta Y}\left(e^{i\beta\Delta Y}-1\right)e^{i\alpha X}}{\Delta Y}-U\frac{De^{i\beta Y}\left(1-e^{-i\alpha\Delta X}\right)e^{i\alpha X}}{\Delta X}-\left(1+\beta^{-1}\right)De^{i\beta Y}K_p e^{i\alpha X}$$

$$\tilde{D}=[1+\{\left(1+\beta^{-1}\right)\frac{2\left(\cos\beta\Delta Y-1\right)}{\left(\Delta Y\right)^2}-M-V\frac{\left(e^{i\beta\Delta Y}-1\right)}{\Delta Y}-U\frac{\left(1-e^{-i\alpha\Delta X}\right)}{\Delta X}-\left(1+\beta^{-1}\right)K_p\}\Delta\tau]D$$
$$+G_r E\Delta\tau+G_m F\Delta\tau$$

$$\therefore\tilde{D}=A_1D+A_2E+A_3F \tag{21}$$

$$A_1=1+\{\left(1+\beta^{-1}\right)\frac{2\left(\cos\beta\Delta Y-1\right)}{\left(\Delta Y\right)^2}-M-V\frac{\left(e^{i\beta\Delta Y}-1\right)}{\Delta Y}-U\frac{\left(1-e^{-i\alpha\Delta X}\right)}{\Delta X}-\left(1+\beta^{-1}\right)K_p\}\Delta\tau$$

$$A_2=G_r\Delta\tau;A_3=G_m\Delta\tau$$

$$\frac{e^{i\alpha X}\left(\tilde{E}-E\right)e^{i\beta Y}}{\Delta\tau}=\left(\frac{1+R_d}{\mathrm{P_r}}\right)\frac{2Ee^{i\alpha X}\left(\cos\beta\Delta Y-1\right)}{\left(\Delta Y\right)^2}e^{i\beta Y}+N_b\frac{Ee^{i\alpha X}\left(e^{i\beta\Delta Y}-1\right)e^{i\beta Y}}{\Delta Y}$$
$$\frac{Fe^{i\alpha X}\left(e^{i\beta\Delta Y}-1\right)e^{i\beta Y}}{\Delta Y}+N_t\left(\frac{Ee^{i\alpha X}\left(e^{i\beta\Delta Y}-1\right)e^{i\beta Y}}{\Delta Y}\right)^2-V\frac{Ge^{i\alpha X}\left(e^{i\beta\Delta Y}-1\right)e^{i\beta Y}}{\Delta Y}$$
$$-U\frac{Ee^{i\alpha X}\left(1-e^{-i\alpha\Delta X}\right)e^{i\beta Y}}{\Delta X}+\left(1+\beta^{-1}\right)E_c\left(\frac{De^{i\alpha X}\left(e^{i\beta\Delta Y}-1\right)e^{i\beta Y}}{\Delta Y}\right)^2+QEe^{i\alpha X}e^{i\beta Y}$$

$$\frac{\left(\tilde{E}-E\right)e^{i\alpha X}e^{i\beta Y}}{\Delta\tau}=\left(\frac{1+R_d}{\mathrm{P_r}}\right)2Ee^{i(\alpha X+\beta Y)}\left(\cos\beta\Delta Y-1\right)\left(\Delta Y\right)^{-2}+N_bEe^{i\alpha X}\left(e^{i\beta\Delta Y}-1\right)e^{i\beta Y}\left(\Delta Y\right)^{-1}$$

$$\frac{F\left(e^{i\beta\Delta Y}-1\right)e^{i\alpha X}e^{i\beta Y}}{\Delta Y}+N_t\left(\frac{Ee^{i\alpha X}\left(e^{i\beta\Delta Y}-1\right)e^{i\beta Y}}{\Delta Y}\right)^2-V\frac{Ge^{i\alpha X}\left(e^{i\beta\Delta Y}-1\right)e^{i\beta Y}}{\Delta Y}$$

$$+\left(1+\beta^{-1}\right)E_c\left(\frac{D\left(e^{i\beta\Delta Y}-1\right)e^{i\alpha X}e^{i\beta Y}}{\Delta Y}\right)^2-U\frac{Ee^{i\alpha X}\left(1-e^{-i\alpha\Delta X}\right)e^{i\beta Y}}{\Delta X}+QEe^{i\alpha X}e^{i\beta Y}$$

$$\tilde{E}=[1+\{\left(\frac{1+R_d}{\mathrm{P_r}}\right)\frac{2\left(\cos\beta\Delta Y-1\right)}{\left(\Delta Y\right)^2}+\left(N_b\phi+N_t\theta\right)\left(e^{i\beta\Delta Y}-1\right)^2\left(\Delta Y\right)^{-2}$$

$$-V\frac{\left(e^{i\beta\Delta Y}-1\right)}{\Delta Y}-U\frac{\left(1-e^{-i\alpha\Delta X}\right)}{\Delta X}+Q\}\Delta\tau]E+\left(1+\beta^{-1}\right)E_cU\frac{\left(e^{i\beta\Delta Y}-1\right)}{\left(\Delta Y\right)^2}D\Delta\tau$$

$$\therefore\tilde{E}=A_4D+A_5E+A_6F \tag{22}$$

$$A_4=\left(1+\beta^{-1}\right)E_cU\frac{\left(e^{i\beta\Delta Y}-1\right)}{\left(\Delta Y\right)^2}\Delta\tau\;;\;A_6=0$$

$$A_5=1+\{\left(\frac{1+R_d}{\mathrm{P_r}}\right)\frac{2\left(\cos\beta\Delta Y-1\right)}{\left(\Delta Y\right)^2}+\left(N_b\phi+N_t\theta\right)\left(e^{i\beta\Delta Y}-1\right)^2\left(\Delta Y\right)^{-2}$$

$$-V\frac{\left(e^{i\beta\Delta Y}-1\right)}{\Delta Y}-U\frac{\left(1-e^{-i\alpha\Delta X}\right)}{\Delta X}+Q\}\Delta\tau$$

$$\frac{\left(\tilde{F}-F\right)e^{i(\alpha X+\beta Y)}}{\Delta\tau}=\frac{1}{L_e}\frac{2Fe^{i\alpha X}\left(\cos\beta\Delta Y-1\right)e^{i\beta Y}}{\left(\Delta Y\right)^2}+\frac{N_t}{N_bL_e}\frac{2e^{i\beta Y}Ee^{i\alpha X}\left(\cos\beta\Delta Y-1\right)}{\left(\Delta Y\right)^2}$$

$$-V\frac{F\left(e^{i\beta\Delta Y}-1\right)e^{i\alpha X}e^{i\beta Y}}{\Delta Y}-U\frac{F\left(1-e^{-i\alpha\Delta X}\right)e^{i\alpha X}e^{i\beta Y}}{\Delta X}-K_r\left(Fe^{i\alpha X}e^{i\beta Y}\right)^p$$

$$\tilde{F}=[1+\{\frac{1}{L_e}\frac{2\left(\cos\beta\Delta Y-1\right)}{\left(\Delta Y\right)^2}-V\frac{\left(e^{i\beta\Delta Y}-1\right)}{\Delta Y}-U\frac{\left(1-e^{-i\alpha\Delta X}\right)}{\Delta X}-K_r\left(\phi\right)^{p-1}\}\Delta\tau]F$$

$$+\frac{N_t}{N_bL_e}\frac{2\Delta\tau\left(\cos\beta\Delta Y-1\right)}{\left(\Delta Y\right)^2}E$$

$$\therefore\tilde{F}=A_7D+A_8E+A_9F \tag{23}$$

$A_7 = 0$; $A_8 = 2N_t\left(N_b L_e\right)^{-1}\left(\cos\beta\Delta Y - 1\right)\Delta\tau\left(\Delta Y\right)^{-2}$

$A_9 = 1 + \{V\left(1 - e^{i\beta\Delta Y}\right)\left(\Delta Y\right)^{-1} - U\left(1 - e^{-i\alpha\Delta X}\right)\left(\Delta X\right)^{-1} + 2\left(L_e\right)^{-1}\left(\cos\beta\Delta Y - 1\right) - K_r\left(\phi\right)^{p-1}\}\Delta\tau$

and these equations (21)-(24) are expressed in matrix notation,

$$\begin{bmatrix} \tilde{D} \\ \tilde{E} \\ \tilde{F} \end{bmatrix} = \begin{bmatrix} A_1 & A_2 & A_3 \\ A_4 & A_5 & A_6 \\ A_7 & A_8 & A_9 \end{bmatrix} \begin{bmatrix} D \\ E \\ F \end{bmatrix} \tag{24}$$

That is, $\tilde{\eta} = \tilde{T}\eta$; where $\tilde{\eta} = \begin{bmatrix} \tilde{D} \\ \tilde{E} \\ \tilde{F} \end{bmatrix}, \tilde{T} = \begin{bmatrix} A_1 & A_2 & A_3 \\ A_4 & A_5 & A_6 \\ A_7 & A_8 & A_9 \end{bmatrix}$ and $\eta = \begin{bmatrix} D \\ E \\ F \end{bmatrix}$

Finding the eigenvalues of the amplification matrix $\tilde{T}$ is necessary to determine the stability condition, but doing so is challenging since the matrix $\tilde{T}$ is a third order square matrix with unique components throughout. The dimensionless time difference $\Delta\tau$ for this explicit finite difference solution is very tiny, tending to zero.

Under this condition, $A_2 = A_3 = A_4 = A_6 \to 0$ and $A_8 \to 0$.

$$\therefore \tilde{T} = \begin{bmatrix} A_1 & 0 & 0 \\ 0 & A_5 & 0 \\ 0 & 0 & A_9 \end{bmatrix}$$

The eigenvalues of the augmentation matrix are generated as $A_1 = \lambda_1, A_5 = \lambda_2$ and $A_9 = \lambda_3$ after simplification. Each eigenvalue's modulus cannot exceed unity for the stability test. The stability criteria are as follows when taking this into account: $|A_1| \le 1, |A_5| \le 1$ and $|A_5| \le 1$.

Let $a_1 = \Delta\tau, a_2 = U\Delta\tau\left(\Delta X\right)^{-1}, a_3 = |-V|\Delta\tau\left(\Delta Y\right)^{-2}$ and $a_4 = 2\Delta\tau\left(\Delta Y\right)^{-2}$. Here, a_1, a_2, a_3 and a_4 are all real and nonnegative. Considering $U = "+"$ and $V = "-"$. Therefore, when $\alpha\Delta X = m_1\pi$ and $\beta\Delta Y = m_2\pi$, with m_1 and m_2 being odd numbers, the highest modulus of A_1, A_5 and A_9 happens.

$$A_1 = 1 - 2\left[\left(1+\beta^{-1}\right)a_4 + M\frac{a_1}{2} + a_2 + a_3 + \left(1+\beta^{-1}\right)\frac{a_1}{2}K_p\right]$$

$$A_5 = 1 - 2\left[\left(\frac{1+R_d}{\mathrm{P_r}}\right)a_4 - N_b a_4\phi - N_t\theta a_4 + a_3 + a_2 - Q\frac{a_1}{2}\right]$$

$$A_9 = 1 - 2\left[\frac{1}{L_e}a_4 + a_3 + a_2 + K_r\left(\phi\right)^{p-1}\frac{a_1}{2}\right]$$

The most detrimental significant value of A_1, A_5 and A_9 is -1.

The stability requirements are as follows:

$$\left(1+\beta^{-1}\right)\frac{2\Delta\tau}{\left(\Delta Y\right)^2} + M\frac{\Delta\tau}{2} + \left|-V\right|\frac{\Delta\tau}{\Delta Y} + U\frac{\Delta\tau}{\Delta X} + \left(1+\beta^{-1}\right)K_p\frac{\Delta\tau}{2} \le 1$$

$$\left(\frac{1+R_d}{\mathrm{P_r}}\right)\frac{2\Delta\tau}{\left(\Delta Y\right)^2} + \left|-V\right|\frac{\Delta\tau}{\Delta Y} - N_t\theta\frac{2\Delta\tau}{\left(\Delta Y\right)^2} - N_b\phi\frac{2\Delta\tau}{\left(\Delta Y\right)^2} + U\frac{\Delta\tau}{\Delta X} + Q\frac{\Delta\tau}{2} \le 1$$

$$\frac{1}{L_e}\frac{2\Delta\tau}{\left(\Delta Y\right)^2} + \left|-V\right|\frac{\Delta\tau}{\Delta Y} + \frac{\Delta\tau}{\Delta X}U + K_r\left(\phi\right)^{p-1}\frac{\Delta\tau}{2} \le 1$$

The primary boundary criterions are $U = V = \theta = \phi = 0$ at $\tau = 0$. For $P_r \ge 0.075$ and $L_e \ge 0.025$, the convergence condition for the present issue would be determined, when $\Delta\tau = 0.0005, \Delta X = 0.80$ and $\Delta Y = 0.20$.

5. Validation of Outcomes

A comparative numerical research with Reza-E-Rabbi et al[45] (Table 2) published work has been shown to verify the evaluation and analyze the veracity of the existing findings. The results have also been validated for the magnetic parameter, Prandtl number, Grashof number, radiation parameter, Lewis number, and Eckert number, and in-depth agreement exists between the recent findings and past findings in the literature. The Figure 4 depicted the comparative study with the Reza-E-Rabbi et al[34] for magnetic parameter. It is observed that there is also great agreement with the result.

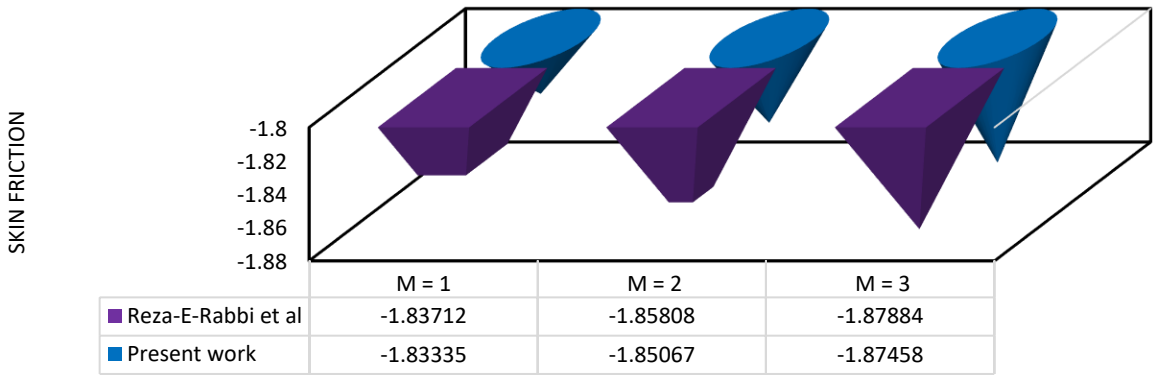

FIGURE 4. Comparative diagram with previous work with respect to Magnetic.

TABLE 2. A tabular comparison of the results with Reza-E-Rabbi et al[45].

Increased Parameter	**Present Result**			**Reza-E-Rabbi et al[45]**		
	U	θ	ϕ	U	θ	ϕ
Magnetic Parameter M	Dec.	Inc.	Inc.	Dec.	-	-
Prandtl number P_r	Dec.	Dec.	Dec.	-	Dec.	-
Grashof number G_r	Inc.	Dec.	Dec.	Inc.	-	-
Heat source parameter Q	Inc.	Inc.	Dec.	-	-	-
Radiation parameter R_d	Inc.	Inc.	Inc.	Inc.	-	-
Lewis number L_e	-	-	Dec.	-	-	Dec.
Eckert number E_c	Inc.	Inc.	Inc.	-	Inc.	-

N.B: Dec. for decrease and Inc. for increase.

6. Results and Discussion

In the involvement of thermal radiation, a heat source, chemical reaction, Brownian motion and thermophoresis, numerical analysis is being done on the non-Newtonian (Casson) MHD fluid flow for free convectional heat and mass transfer past on a vertical, infinitely permeable plate. The numerical outcomes of velocity (U), temperature (θ), and concentration (ϕ) are generated for various parameters in order to understand the actual physical representation of the problem when boundary layer conditions are present. The graphs are represented with some constant parameter G_r = 4.00, G_m = 2.00, M = 1.00, P_r = 0.71, L_e = 5.00, N_b = 0.10, R_d = 2.00, E_c = 0.10, β = 0.10, K_p = 0.40, N_t = 0.10, A = 0.50, P = 2.00, Q = 0.10, K_r = 5.00.

Velocity Field

The physical behavior of the magnetic parameter, *M*, for velocity fields is shown in Figure 5. When a magnetic field is present in a system, the Lorentz force is created. This force slows down the motion of the fluid. The impacts of Prandtl number, *Pr*, on velocity distribution is depicted in Figure 6. It is shown that when the Prandtl number rises, velocity decreases. *Pr* quantifies the correlation between thermal and momentum diffusivity. *Pr* regulates the relative momentum and thickness of momentum boundary layer. A rise in the Prandtl number, for a certain amount of specific heat capacity and thermal conductivity, merely denotes an increase in the degree of fluid viscosity. Fluids with low velocity are those whose viscosity value is high.

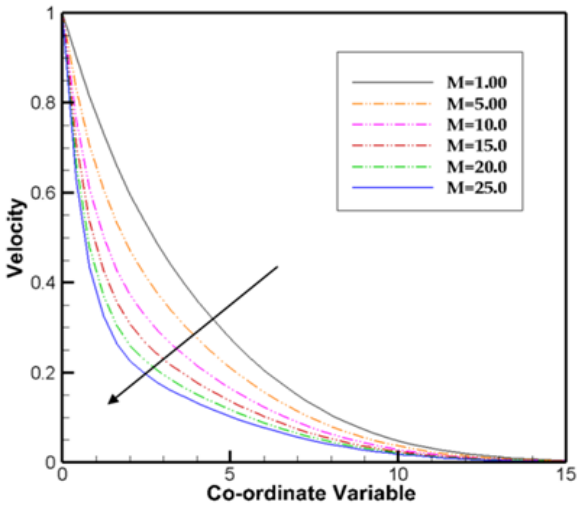

FIGURE 5. The influence of *M* on *U*.

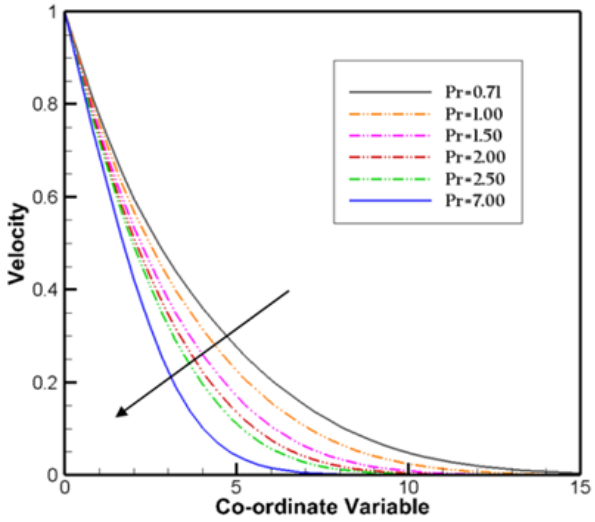

FIGURE 6. The impact of P_r on *U*.

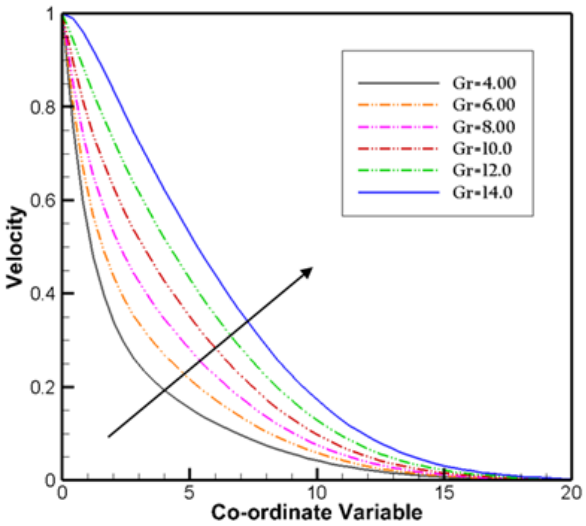

FIGURE 7. The effect of G_r on *U*.

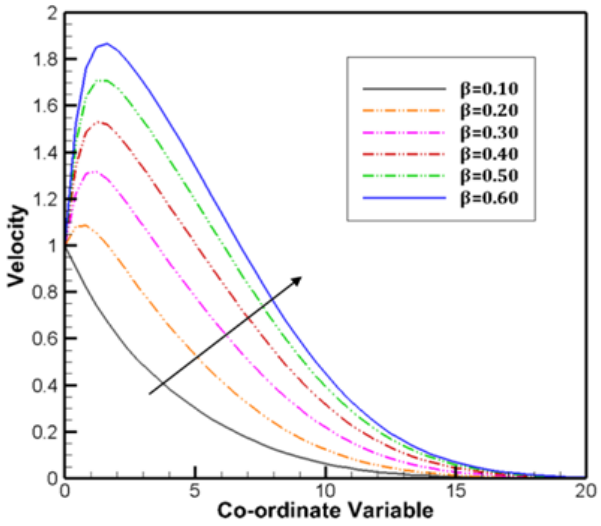

FIGURE 8. The impact of β on *U*.

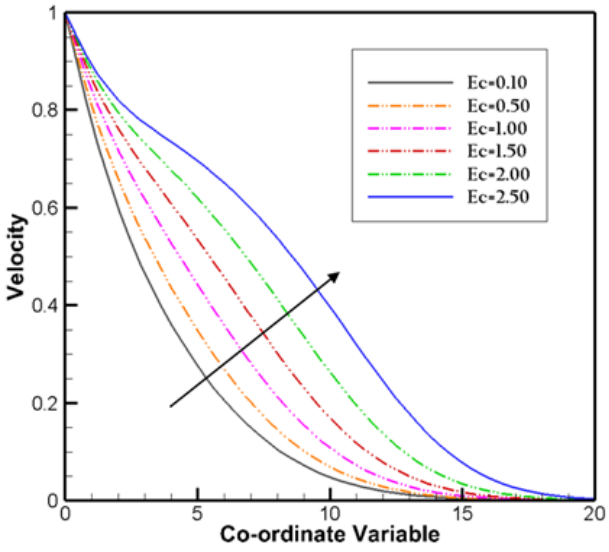

FIGURE 9. The impression of E_c on.

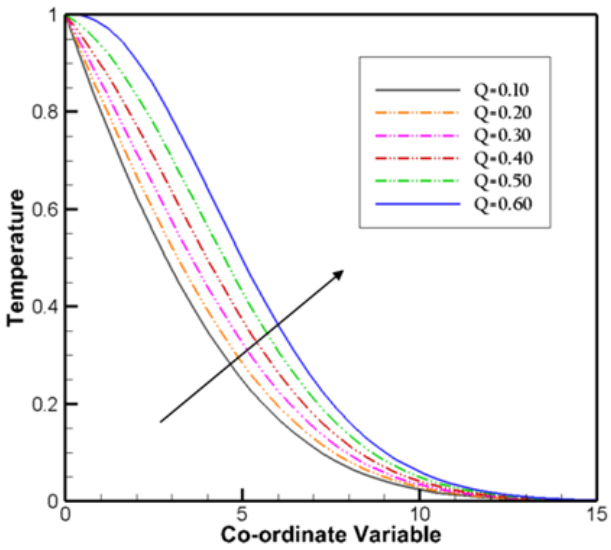

FIGURE 10. The impact of Q on θ.

Figure 7 represents the variation in the velocity profile caused by Thermal Grashof number (Gr). As the parameter increases, the velocity increases. Generally speaking, increasing a buoyancy parameter makes buoyant forces more dominant in the flow, helping to enhance more particle contact and increasing the velocity field. The impact of Casson parameter is presented in Figure 8. The greater viscous forces acting on the flow when the Casson fluid is incorporated are the cause of this tendency and can contribute to the velocity depreciation. The influence of Eckert number (Ec) is depicted in Figure 9. Eckert is the ratio of advective mass transport to heat dissipation. So, for the increase of Eckert number, velocity rises.

Temperature Field

In many industry processes, thermal radiation is the important one. So, it is a great deal by knowing the impacts of different pertinent parameter on temperature profiles. Figure 10 displays the heat source parameter (Q). As the heat source parameter is improved, temperature rises. Figure 11 illustrates how Eckert number (E_c) works. The particles become active and produce a greater temperature as a result of the energy storage at high Eckert numbers. Additionally in Figure 12, the temperature distribution has also been shown for Prandtl number (P_r). Thermal conductivities are higher in fluids with lower (P_r). So, compare to greater number, heat will diffuse from the sheet more quickly. Hence, the use of Prandtl number can accelerate cooling in conducting fluids. Figure 13 displays the distribution in the temperature profile brought on by the radiation parameter (Rd).

It demonstrates that higher values of the radiation parameter result in higher temperatures and correspondingly thicker thermal boundary layers. Higher values of radiation typically result in operating fluid heating up more, which raises the temperature of the surrounding area.

Concentration Field

The Lewis number is used to figure out the relative thickness between the thermal and concentration boundary layers. The purpose of Figure 14 is to investigate how the Lewis number (*Le*) affects the concentration profile.

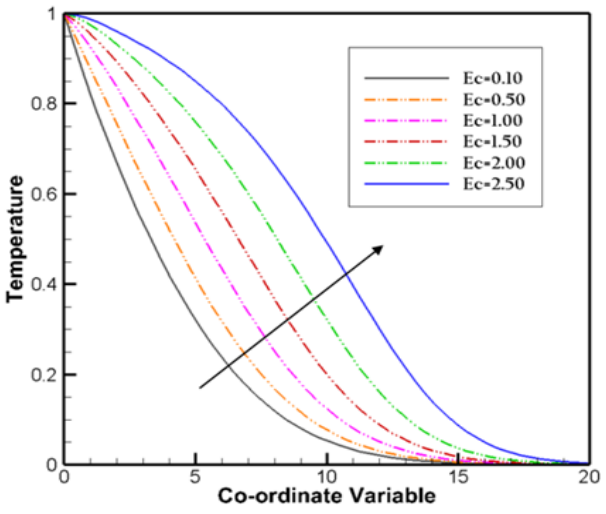

FIGURE 11. The effect of E_c on θ.

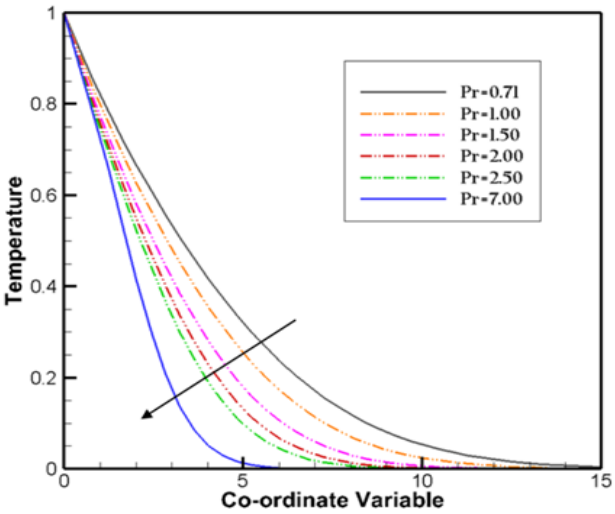

FIGURE 12. The impact of P_r on θ.

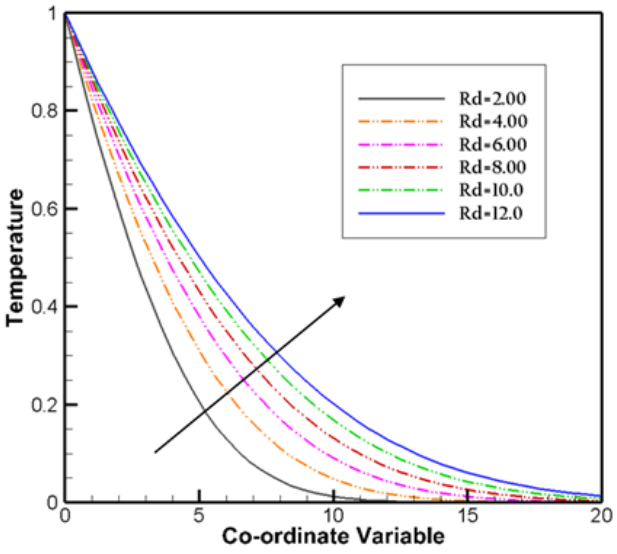

FIGURE 13. The influence of R_d on θ.

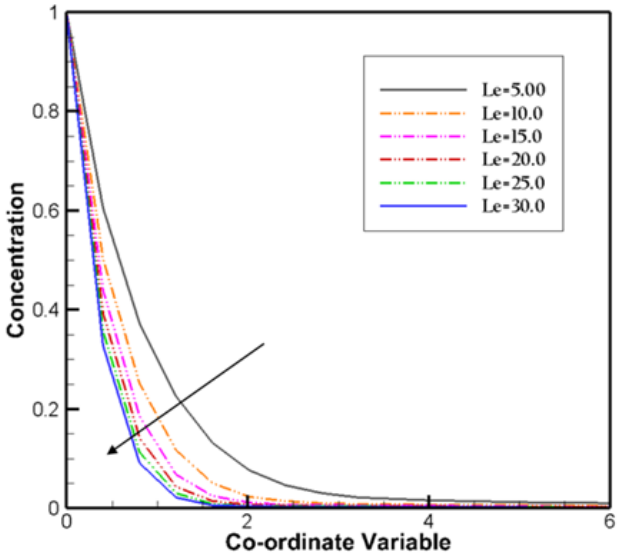

FIGURE 14. The impact of L_e on ϕ.

If concentration boundary layer thickness increases, then there is a decrement of Lewis number. Figure 14 demonstrates that the heat expands quicker than the solute when $L_e > 5.0$. Thermophoresis parameter creates an impact on concentration which is shown in Figure 15. Temperature gradients cause the transport force known as thermophoresis parameter to exist. So, due to the increasing values of it there is also an increase of concentration. Figure 16 describes the influence of Casson parameter on concentration field. Casson parameter values that increase over time produce an increasing profile. Physically, the fluid's viscosity causes the fluid's velocity to slow down, saturating the nanoparticles close to the stretched sheet.

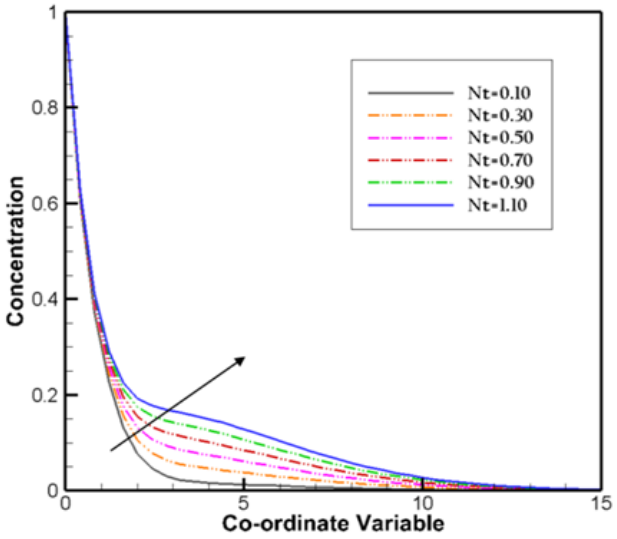

FIGURE 15. The impression of N_t on ϕ.

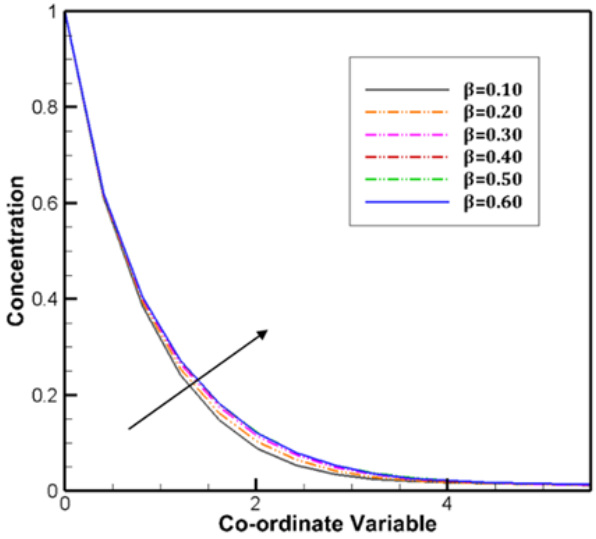

FIGURE 16. The impact of β on ϕ.

Skin friction, Nusselt and Sherwood Numbers

Figure 17 illustrates how a magnetic parameter affects skin friction and describes that magnetic parameter tends to reduce the stress, which causes the fluid velocity to slow down. Added to that Figures 23 and 24 have shown the influence of parameter for chemical change and Lewis number on Sherwood number respectively. It has been seen that the effect of both parameter for chemical change and the Lewis number cause the Sherwood number to increase. The action of skin friction under the influence of porosity term has been depicted in Figure 18.

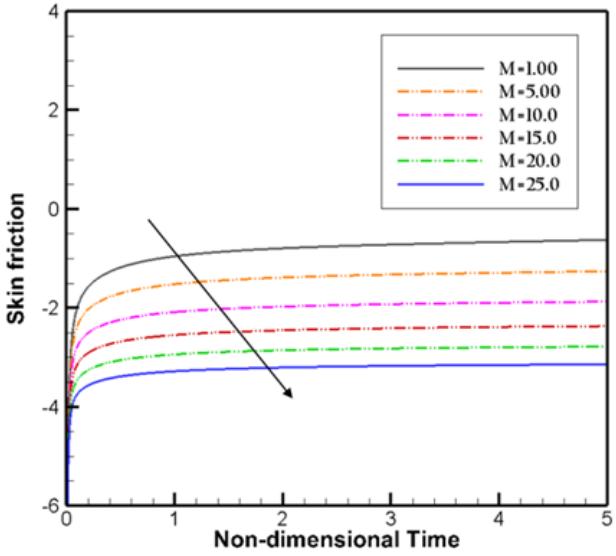

FIGURE 17. The influence of M on C_f.

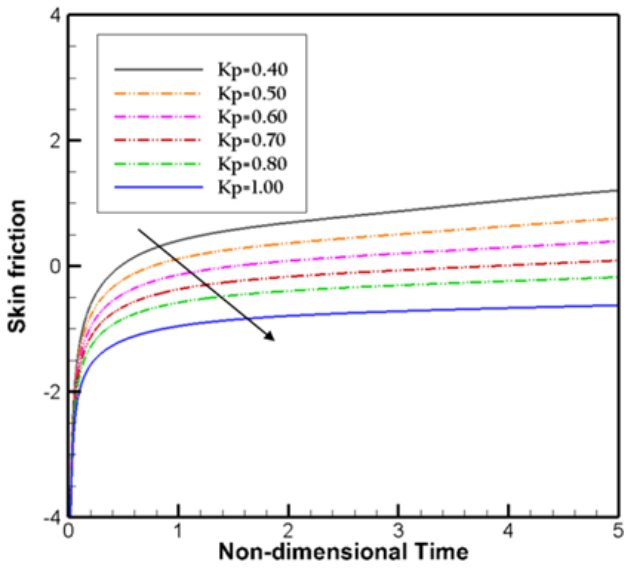

FIGURE 18. The impact of K_p on C_f.

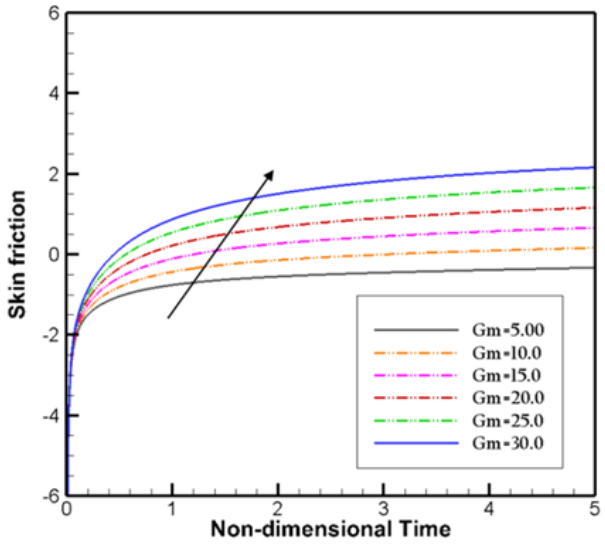

FIGURE 19. The influence of G_m on C_f.

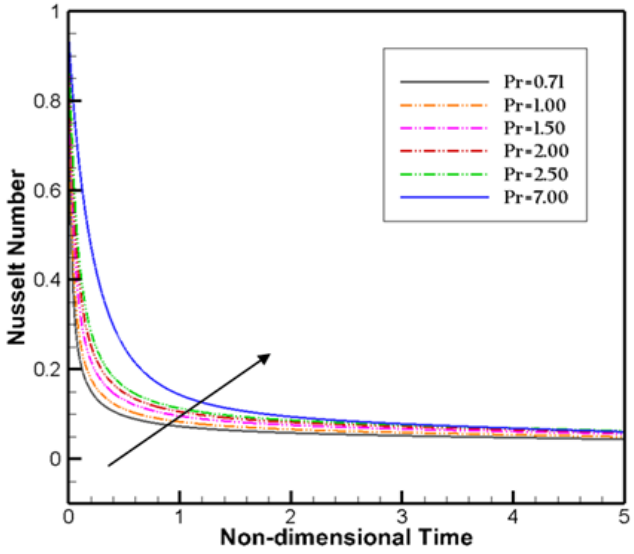

FIGURE 20. The impact of P_r on N_u.

It has been observed that with the increase of porosity term, skin friction decreases. Impact of Grashof number on skin friction is demonstrated in Figure 19. In addition, Figures 20-22 highlight the Prandtl number, magnetic parameter and Grashof number on Nusselt number respectively. It has been noted that Prandtl number causes an increase in Nusselt number, while magnetic parameter and Grashof number cause a drop.

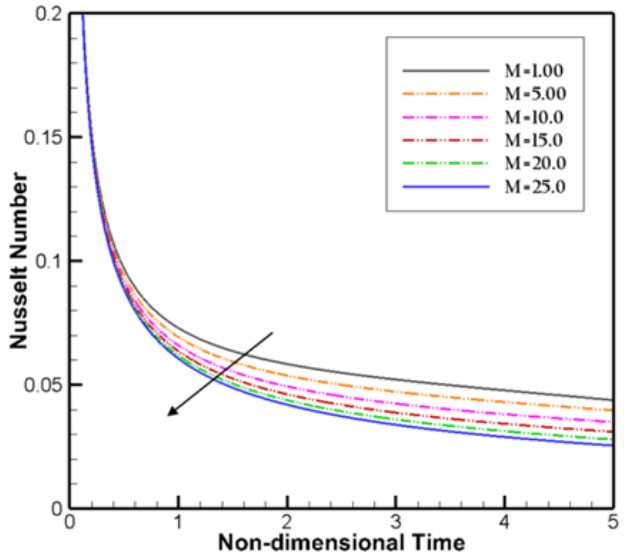

FIGURE 21. The impact of M on N_u.

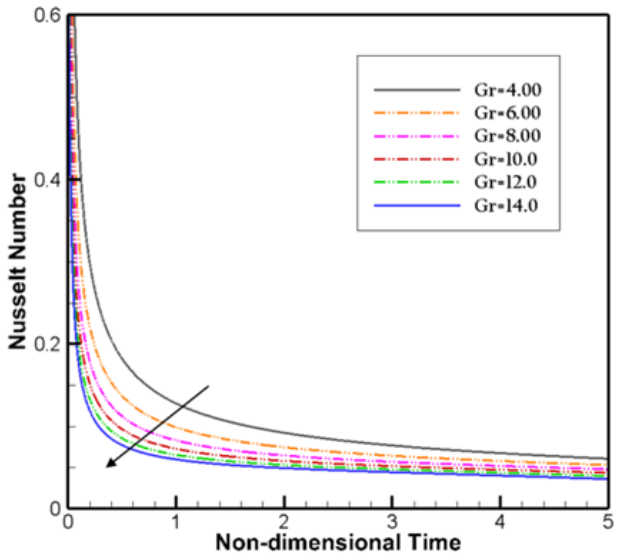

FIGURE 22. The impact of G_r on N_u.

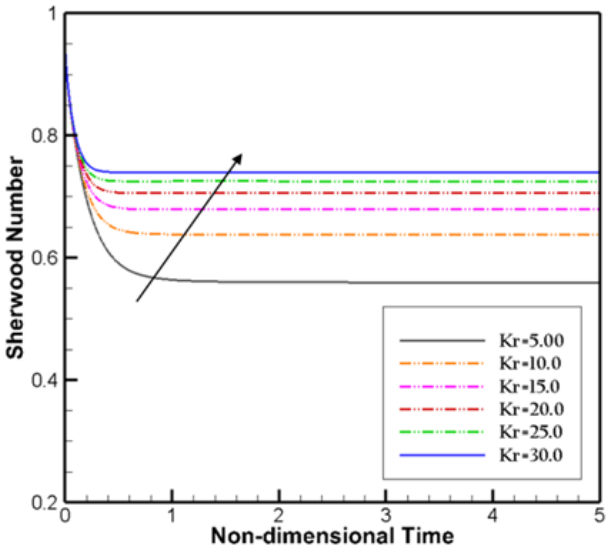

FIGURE 23. The impact of K_r on S_h.

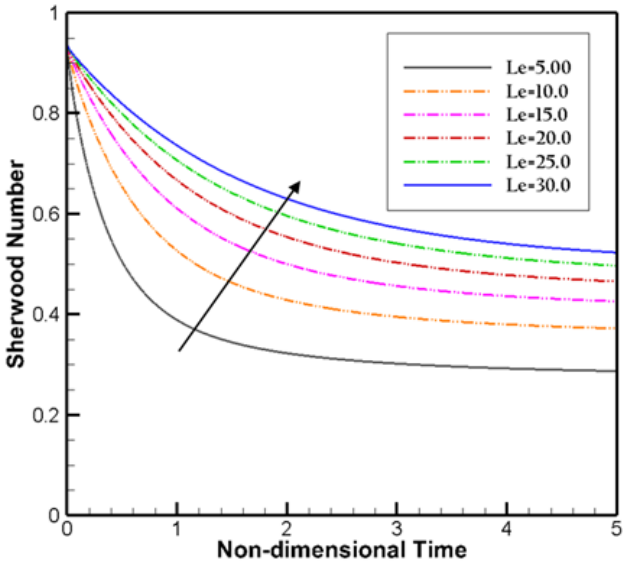

FIGURE 24. The impact of L_e on S_h.

Streamlines and Isothermal Lines

Figures 25-28 show an improved picture of fluid movement. Here, a streamline depicts the direction of the fluid's velocity. For changing the quantities of the thermal Grashof number and radiation parameter, both the flood view and the line view of the fluid flow have been provided here. However, isotherms can be employed to show how the thermal boundary layer varies. Figures 25-28 show both streamlines' and isotherms' overall impressions. Streamlines and isotherms both decline as both parameters are increased.

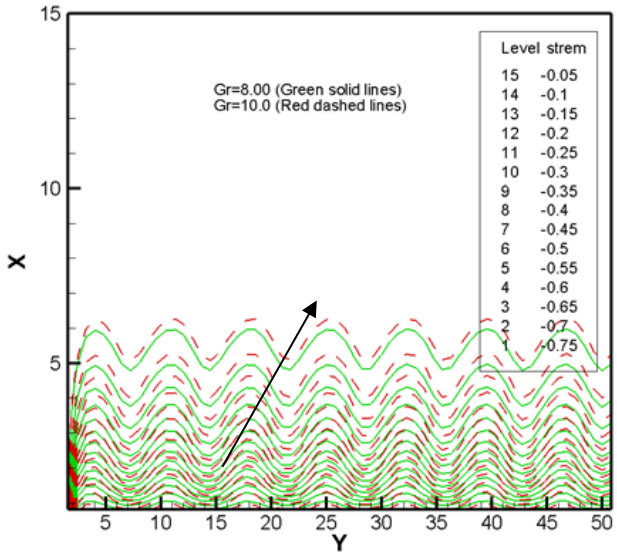

FIGURE 25. Streamlines for different values of G_r (line view).

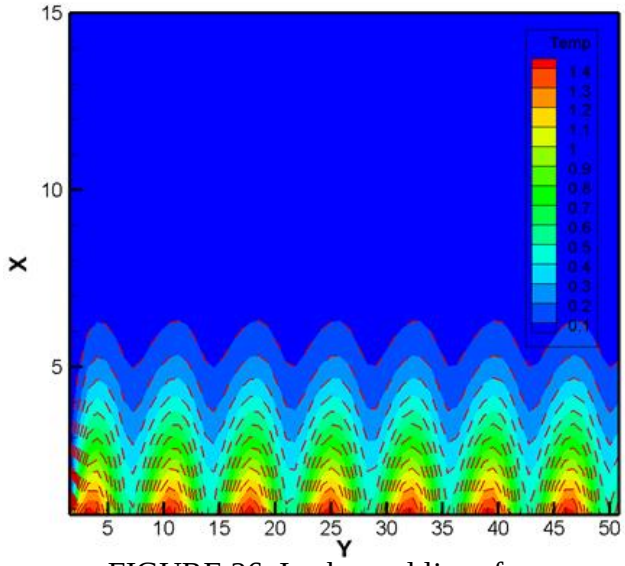

FIGURE 26. Isothermal lines for several values of G_r (flood view).

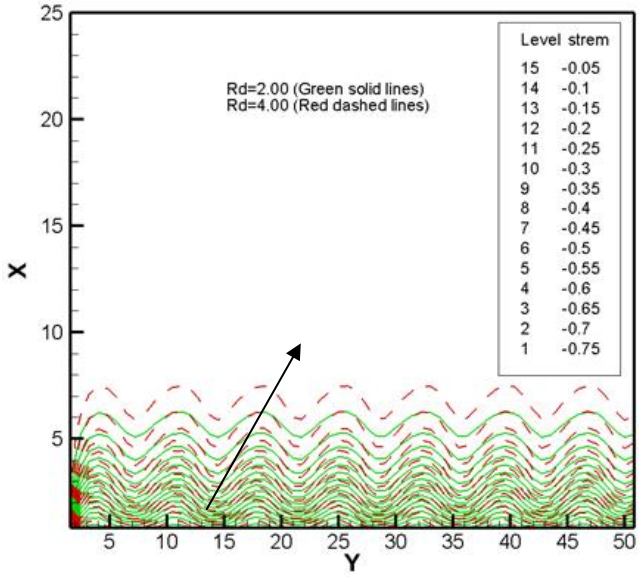

FIGURE 27. Streamlines for several values of R_d (line view).

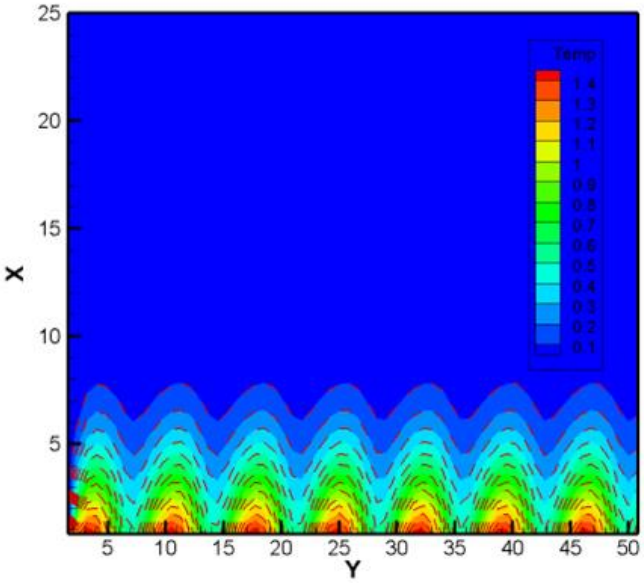

FIGURE 28. Isothermal lines for different values of R_d (flood view).

Curve to curve fluctuation of M, P_r and Ec for a steady-state solution at $\tau = 3.50$ is presented in Table 3 and also the effect of M, P_r, G_r, G_m, R_d, L_e, E_c, Q and β on Sherwood number (S_h), Nusselt number (N_u) and skin friction (C_f) at $\tau = 2.00$ described in Table 4.

TABLE 3. Curve to curve fluctuation of M, P_r and E_c for a steady-state solution at $\tau = 3.50$.

Increased Parameter	Velocity Profile (U)	Inc. or Dec.	Temperature Profile (θ)	Inc. or Dec.	Concentration Profile (ϕ)	Inc. or Dec.
M						
1.00	0.08895	**Dec.**	0.10012	**Inc.**	0.00440	**Inc.**
5.00	0.06754	24.00%	0.10272	2.60%	0.00454	3.18%
10.0	0.05328	21.60%	0.10748	4.63%	0.00475	4.63%
P_r						
0.71	0.08895	**Dec.**	0.10012	**Dec.**	0.00440	**Dec.**
1.00	0.05355	39.80%	0.05584	44.23%	0.00359	18.41%
1.50	0.02532	52.72%	0.02195	60.69%	0.00223	37.88%
E_c						
0.10	0.08895	**Inc.**	0.10012	**Inc.**	0.00440	**Inc.**
0.50	0.12424	39.67%	0.14234	42.17%	0.00584	32.73%
1.00	0.18473	48.69%	0.21737	52.71%	0.00768	31.50%

TABLE 4. Effect of M, P_r, G_r, G_m, R_d, L_e, E_c, Q and β on Sherwood number (S_h), Nusselt number (N_u) and skin friction (C_f) at $\tau = 2.00$.

M	P_r	G_r	G_m	R_d	L_e	E_c	Q	β	C_f	N_u	S_h
1.00	0.71	4.00	2.00	2.00	5.00	0.10	0.10	0.10	-0.79051	0.05847	0.32306
5.00	-	-	-	-	-	-	-	-	-1.38221	0.05382	0.32401
7.00	-	-	-	-	-	-	-	-	-1.63335	0.05191	0.32437
-	**0.71**	-	-	-	-	-	-	-	-0.79051	0.05847	0.32306
-	**1.00**	-	-	-	-	-	-	-	-0.84641	0.06639	0.32183
-	**2.00**	-	-	-	-	-	-	-	-0.96268	0.08234	0.31980
-	-	**4.00**	-	-	-	-	-	-	-3.90821	0.09240	0.64086
-	-	**6.00**	-	-	-	-	-	-	-2.36044	0.07473	0.47324
-	-	**8.00**	-	-	-	-	-	-	-1.48791	0.06484	0.38175

-	-	-	**2.00**	-	-	-	-	-	- 0.79051	0.05847	0.32306
-	-	-	**5.00**	-	-	-	-	-	- 0.54572	0.05892	0.32275
-	-	-	**10.0**	-	-	-	-	-	- 0.13687	0.05958	0.32225
-	-	-	-	**2.00**	-	-	-	-	- 0.91276	0.05824	0.32321
-	-	-	-	**4.00**	-	-	-	-	- 0.83334	0.04738	0.32492
-	-	-	-	**6.00**	-	-	-	-	- 0.78590	0.04099	0.32590
-	-	-	-	-	**5.00**	-	-	-	- 0.79051	0.05847	0.32306
-	-	-	-	-	**10.0**	-	-	-	- 0.83487	0.05834	0.42878
-	-	-	-	-	**15.0**	-	-	-	- 0.85851	0.05834	0.50037
-	-	-	-	-	-	**0.10**	-	-	- 0.79051	0.05847	0.32306
-	-	-	-	-	-	**0.30**	-	-	- 0.72833	0.04630	0.32785
-	-	-	-	-	-	**0.50**	-	-	- 0.67284	0.03624	0.33171
-	-	-	-	-	-	-	**0.10**	-	- 0.79051	0.05847	0.32306
-	-	-	-	-	-	-	**0.20**	-	- 0.74611	0.04989	0.32483
-	-	-	-	-	-	-	**0.30**	-	- 0.69778	0.04071	0.32663
-	-	-	-	-	-	-	-	**0.10**	- 0.79051	0.05847	0.32306
-	-	-	-	-	-	-	-	**0.20**	0.28606	0.06892	0.32338
-	-	-	-	-	-	-	-	**0.30**	0.61236	0.07306	0.32367

7. Conclusions

In this paper, an unstable MHD convective flow of non-Newtonian (Casson) fluid through an unlimited vertical plate having sinusoidal boundary conditions has been examined in the vicinity of chemical reaction as well as thermal radiation. Modeling PDEs with appropriate technique was solved using EFD. To make sure the solution was stable, a convergence evaluation was performed. Additionally, it was proven that the current outcomes are independent of the grid. Additionally, the current numerical model has been validated using previously published findings. The primary conclusions yielded from the aforesaid study are as follows:

1. While the magnetic factor and the Prandtl number have slowed the velocity profile, the existence of an Eckert number, Grashof number and Casson parameter has significantly increased the velocity.
2. For the heat source parameter, radiation parameter, and Eckert number, there is an increase in heat.
3. Lewis number causes a fall in the concentration profile, whereas thermophoresis parameter and Casson fluid parameter cause increases.
4. Both chemical reaction parameter and the Lewis number cause the Sherwood number to increase.
5. Prandtl number causes an increase in Nusselt number, while magnetic parameter and Grashof number cause a drop.
6. The increase of porosity term decreases the skin friction.

Conflict of Interest

The authors declare no potential conflict of interest.

References

1. Saqib M, Ali F, Khan I, Sheikh NA. Heat and mass transfer phenomena in the flow of Casson fluid over an infinite oscillating plate in the presence of first-order chemical reaction and slip effect. *Neural Comp Appli.* 2016
2. Hussanan A, Salleh MZ, Tahar RM, Khan I. Unsteady Boundary Layer Flow and Heat Transfer of a Casson Fluid past an Oscillating Vertical Plate with Newtonian Heating. *PLoS ONE.* 2014;9(10):e108763.

3. Rafique K, Anwar MI, Misiran M, Khan I, Alharbi SO, Thounthong P, Nisar KS. Numerical Solution of Casson Nanofluid Flow Over a Non-linear Inclined Surface With Soret and Dufour Effects by Keller-Box Method. *Front Phys.* 2019;7:139.
4. Raju CSK, Sandeep N, Sugunamma V, Babu JM, Reddy RJV. Heat and mass transfer in magnetohydrodynamic Casson fluid over an exponentially permeable stretching surface. *Eng Sci Tech Int J.* 2016;19(1);45–52.
5. Asogwa KK, Ibe AA. A Study of MHD Casson Fluid Flow over a Permeable Stretching Sheet with Heat and Mass Transfer. *J Eng Rese Rep.* 2020;16(2):10-25.
6. Rao EM. The effects of thermal radiation and chemical reaction on MHD flow of a Casson fluid over and exponentially inclined stretching surface. *J Phys: Conference Series*. 2018;1000;012158
7. Sarker T, Reza-E-Rabbi S, Arifuzzaman SM, Ahmed R, Khan MS, Ahmmed SF. MHD Radiative Flow of Casson and Williamson Nanofluids over an Inclined Cylindrical Surface with Chemical Reaction Effects. *Int J Heat Tech*. 2019;37(4);1117-1126.
8. Ullah I, Bhattacharyya K, Shafie S, Khan I. Unsteady MHD Mixed Convection Slip Flow of Casson Fluid over Nonlinearly Stretching Sheet Embedded in a Porous Medium with Chemical Reaction, Thermal Radiation, Heat Generation/ Absorption and Convective Boundary Conditions. *PLoS ONE.* 2016;11(10):e0165348.
9. Hasnain J, Abbas Z, Sheikh M, Aly S. Analysis of dusty Casson fluid flow past a permeable stretching sheet bearing power law temperature and magnetic field. *Int J Num Methods Heat Fluid Flow.* 2019;30(6);3463–3480
10. Pramanik S. Casson fluid flow and heat transfer past an exponentially porous stretching surface in presence of thermal radiation. *Ain Shams Eng J.* 2014;5(1);205–212
11. Oke AS, Mutuku WN, Kimathi M, Animasaun IL. Insight into the dynamics of non-Newtonian Casson fluid over a rotating non-uniform surface subject to Coriolis force. *Nonlinear Eng*. 2020;9(1);398–411
12. Sulochana C, Poornima M. Unsteady MHD Casson fluid flow through vertical plate in the presence of Hall current. *SN App Sci.* 2019;1(12).
13. Zaib A, Bhattacharyya K, Uddin MS, Shafie S. Dual Solutions of Non-Newtonian Casson Fluid Flow and Heat Transfer over an Exponentially Permeable Shrinking Sheet with Viscous Dissipation. *Model Simul Eng.* 2016;1–8.

14. Sohail M, Shah Z, Tassaddiq A, Kumam P, Roy P. Entropy generation in MHD Casson fluid flow with variable heat conductance and thermal conductivity over non-linear bi-directional stretching surface. *Sci Rep.* 2020;10(1).
15. Mondal RK, Reza-E-Rabbi S, Gharami PP, Ahmmed SF, Arifuzzaman SM. A Simulation of Casson Fluid Flow with Variable Viscosity and Thermal Conductivity Effects. *Math Model Eng Prob*. 2019;6(4);625-633.
16. Abro KA, Shaikh HS, Khan I. A mathematical Study of Magnetohydrodynamic Casson Fluid via Special Functions with Heat and Mass Transfer embedded in Porous Plate. arXiv:1706.03829 (physics). 2017;
17. Prameela M, Gangadhar K, Reddy GJ. MHD free convective non-Newtonian Casson fluid flow over an oscillating vertical plate. *Part Diff Equ App Math.* 2022;5;100366.
18. Ogunseye HA, Salawu SO, Fatunmbi EO. A numerical study of MHD heat and mass transfer of a reactive Casson–Williamson nanofluid past a vertical moving cylinder. *Part Diff Equ App Math.* 2021;4;100148
19. Asogwa KK, Goud BK, Reddy BS, Ibe AA. Suction effect on the dynamics of EMHD casson nanofluid over an induced stagnation point flow of stretchable electromagnetic plate with radiation and chemical reaction. *Resu Eng.* 2022;15;100518
20. Khalid A, Khan I, Khan A, Shafie S. Unsteady MHD free convection flow of Casson fluid past over an oscillating vertical plate embedded in a porous medium. *Eng Sci Tech Int J.* 2015;18;309e317
21. Kumar KG, Archana M, Gireesha BJ, Krishanamurthy MR, Rudraswamy NG. Cross diffusion effect on MHD mixed convection flow of nonlinear radiative heat and mass transfer of Casson fluid over a vertical plate. *Resu Phys.* 2018;8:694–701
22. Qayyum M, Khan H, Khan O. Slip Analysis at Fluid-Solid Interface in MHD Squeezing Flow of Casson Fluid through Porous Medium. *Resu Phys*. 2017;7:732–750
23. Reddy GJ, Raju RS, Rao JA. Influence of viscous dissipation on unsteady MHD natural convective flow of Casson fluid over an oscillating vertical plate via FEM. *Ain Shams Eng J*. 2018;9:1907–1915
24. Shoaib M, Kausar M, Nisar KS, Raja MAZ, Morsy A. Impact of thermal energy on MHD Casson fluid through a Forchheimer porous medium with inclined non-linear surface: A soft computing approach. *Alex Engi J*. 2022; 61:12211–12228

25. Bejawada SG, Reddy YD, Jamshed W, Nisar KS, Alharbi AN, Chouikh R. Radiation effect on MHD Casson fluid flow over an inclined non-linear surface with chemical reaction in a Forchheimer porous medium. *Alex Eng J*. 2022;61:8207–8220
26. Kataria HR, Patel HR. Radiation and chemical reaction effects on MHD Casson fluid flow past an oscillating vertical plate embedded in porous medium. *Alex Eng J*. 2016;55:583–595
27. Animasaun IL, Adebile EA, Fagbade AI. Casson fluid flow with variable thermo-physical property along exponentially stretching sheet with suction and exponentially decaying internal heat generation using the homotopy analysis method. *J Nigerian Math Soci*. 2016;35:1–17
28. Khan MR, Elkotb MA, Matoog RT, Alshehri NA, Abdelmohimen MAH. Thermal features and heat transfer enhancement of a Casson fluid across a porous stretching/shrinking sheet: Analysis of dual solutions. *Case Stud Therm Eng.* 2021;28:101594
29. Hussain F, Nazeer M, Altanji M, Saleem A, Ghafar MM. Thermal analysis of Casson rheological fluid with gold nanoparticles under the impact of gravitational and magnetic forces. *Case Stud Therm Eng*. 2021;28:101433
30. Zhou JC, Abidi A, Shi QH, Khan MR, Rehman A, Issakhov A, Galal AM. Unsteady radiative slip flow of MHD Casson fluid over a permeable stretched surface subject to a non-uniform heat source. *Case Stud Therm Eng*. 2021;26:101141
31. Rasool G, Chamkha AJ, Muhammad T, Shafiq A, Khan I. Darcy-Forchheimer relation in Casson type MHD nanofluid flow over non-linear stretching surface. *Prop Power Rese.* 2020;9(2):159e168
32. Raju CSK, Neeraja G, Dinesh PA, Vidya K, Rushi Kumar B. MHD Casson fluid in a suspension of convective conditions and cross diffusion across a surface of paraboloid of revolution. *Alex Eng J.* 2018;xxx;xxx–xxx
33. Saidulu N, Lakshmi AV. MHD Flow of Casson Fluid With Slip Effects over an Exponentially Porous Stretching Sheet in Presence of Thermal Radiation, Viscous Dissipation and Heat Source/Sink. *ARJM*, ISSN(online), 2016;15(2);2378-704X
34. Reza-E-Rabbi S, Ahmmed SF, Islam S, Arifuzzaman SM, Rana BMJ, Yousuf Ali M, Al-Mamun A, Khan MS. Characterization of fluid flow and heat transfer of a periodic magnetohydrodynamics nano non-Newtonian liquid with Arrhenius activation energy and nonlinear radiation. *Heat Transf.* 2022;1-38;Wiley.

35. Anwar T, Kumam P, Watthayu W. Unsteady MHD natural convection flow of Casson fluid incorporating thermal radiative flux and heat injection/suction mechanism under variable wall conditions. *Sci Rep.* 2021;11(1)
36. Moatimid GM, Mohamed MAA, Elagamy K. A Casson nanofluid flow within the conical gap between rotating surfaces of a cone and a horizontal disc. *Sci Rep.* 2022;12:11275
37. Ahmad S, Haq SU, Ali F, Khan I, Nisar KS. Time fractional analysis of channel flow of couple stress Casson fluid using Fick's and Fourier's Laws. *Sci Rep.* 2022;12:2956
38. Sohail M, Shah Z, Tassaddiq A, Kumam P, Roy P. Entropy generation in MHD Casson fluid flow with variable heat conductance and thermal conductivity over non-linear bi-directional stretching surface. *Sci Rep.* 2020;10(1);10:12530
39. Sahoo A, Nandkeolyar R. Entropy generation and dissipative heat transfer analysis of mixed convective hydromagnetic flow of a Casson nanofluid with thermal radiation and Hall current. *Sci Rep.* 2021;11(1);11:3926
40. Shah Z, Kumam P, Deebani W. Radiative MHD Casson Nanofluid Flow with Activation energy and chemical reaction over past nonlinearly stretching surface through Entropy generation. *Sci Rep.* 2020;10(1);10:4402
41. Kataria HR, Patel HR. Heat and mass transfer in magnetohydrodynamic (MHD) Casson fluid flow past over an oscillating vertical plate embedded in porous medium with ramped wall temperature. *Prop Power Rese.* 2018;7(3);257–267.
42. Ali A, Umar M, Bukhari Z, Abbas Z. Pulsating flow of a micropolar-Casson fluid through a constricted channel influenced by a magnetic field and Darcian porous medium: A numerical study. *Res Phys.* 2020;19;103544
43. Hussain M, Ghaffar A, Ali A, Shahzad A, Nisar KS, Alharthi MR, Jamshed W. MHD thermal boundary layer flow of a Casson fluid over a penetrable stretching wedge in the existence of nonlinear radiation and convective boundary condition. *Alex Eng J.* 2021;60;5473–5483
44. Nandeppanavar MM, Vaishali S, Kemparaju MC, Raveendra, N. Theoretical analysis of thermal characteristics of casson nano fluid flow past an exponential stretching sheet in Darcy porous media. *Case Stud Therm Eng.* 2020;21;100717
45. Reza-E-Rabbi S, Ahmmed SF, Arifuzzaman SM, Sarkar T, Khan MS. Computational modelling of multiphase fluid flow behaviour over a stretching sheet in the presence of nanoparticles. *Eng Sci Tech Int J.* 2020;23;605–617